JOURNAL OF GEOPHYSICAL RESEARCH, VOL. 97, NO. B2, PAGES 1921–1942, FEBRUARY 10, 1992

Thin, Low-Velocity Crust Beneath the Southern Yukon-Tanana Terrane, East Central Alaska: Results From Trans-Alaska Crustal Transect Refraction/Wide-Angle Reflection Data

BRUCE C. BEAUDOIN

U.S. Geological Survey, Menlo Park, California
and Department of Geophysics, Stanford University, Stanford, California

GARY S. FUIS, WALTER D. MOONEY, AND WARREN J. NOKLEBERG

U.S. Geological Survey, Menlo Park, California

NIKOLAS I. CHRISTENSEN

Department of Earth and Atmospheric Sciences, Purdue University, West Lafayette, Indiana

A seismic refraction/wide-angle reflection survey for the Trans-Alaska Crustal Transect program reveals a thin, reflective crust beneath the southern Yukon-Tanana terrane (YTT) in east central Alaska. These data are the first detailed refraction survey of the southern YTT and compose a 130-km-long reversed profile along the Alaska and Richardson highways. Results from this study indicate that low-velocity ($\leq$ 6.4 km/s) rocks extend to approximately 27 km in depth. Based on these low velocities and an average Poisson's ratio of 0.23 determined for depths of $\leq$ 27 km, an overall silicic composition is interpreted for this portion of the crust beneath the Yukon-Tanana terrane. From approximately 8 to 27 km depth the crust exhibits an increase in reflectivity. This middle to lower crustal reflectivity is modeled as alternating high- and low-velocity lamellae with an average velocity of 6.1 km/s at 10 km depth to an average velocity of 6.4 km/s at 27 km depth. Beneath these reflective, low-velocity rocks a 3- to 5-km-thick, 7.0 km/s basal crustal layer produces a prominent reflection that extends to offsets of up to 280 km. The crust-mantle boundary, modeled at an average depth of 30 km, produces a variable *PmP* reflection, which may indicate lateral heterogeneity of this boundary, and a weak and emergent *Pn* refraction with a velocity of 8.2 km/s. We interpret the crustal section as follows: the low-velocity rocks of the southern YTT extend from the surface to depths of approximately 10 km; underthrust Mesozoic flysch of the Kahiltna terrane, rocks of the Gravina arc, and basement of the Wrangellia(?) terrane extend from 10 to 27 km depth; a 3- to 5-km-thick layer of mantle-derived mafic rocks, relic oceanic crust, or Wrangellia(?) terrane lower crust extends from 27 to approximately 30 km depth; a tectonically young Moho beneath the southern YTT is found at an average depth of 30 km; and it is underlain by a mantle that may be relatively cool and/or olivine rich. In this interpretation, the Yukon-Tanana terrane is a thin-skinned terrane. Our results indicate that tectonic, and possibly magmatic, underplating has played a significant role in crustal growth for central Alaska.

INTRODUCTION

The division of the North American Cordillera into tectonostratigraphic terranes [*Coney et al.*, 1981; *Jones et al.*, 1982; *Monger*, 1984] has provided a framework for developing an accretionary history along the continental margin. Alaska, with its plethora of allochthonous terranes, has proven useful in this endeavor. To investigate the structure, composition, and evolution of the Alaskan crust, the U.S. Geological Survey (USGS) initiated the Trans-Alaska Crustal Transect (TACT) program in 1984 [*Page et al.*, 1986]. The TACT program is a multidisciplinary investigation of the tectonostratigraphic terranes that compose the Alaskan lithosphere from Valdez to Prudhoe Bay along the Trans-Alaska Pipeline system and across the adjacent Pacific and Arctic Alaskan continental margins. Results from this program and other studies reveal significant geologic differences [e.g., *Plafker et al.*, 1989*a*] as well as geophysical differences [*Barnes*, 1977; *Campbell and Nokleberg*, 1986; *Campbell*, 1987; *Labson et al.*, 1988; *Stanley et al.*, 1990] between terranes. Seismically, terranes traversed by TACT also exhibit unique reflection and velocity structures [e.g., *Brocher et al.*, 1989; *Fisher et al.*, 1989; *Goodwin et al.*, 1989, *Fuis et al.*, 1991].

This paper presents TACT refraction results from the southern Yukon-Tanana terrane (YTT) in east central Alaska. During the summer of 1987 the USGS, in cooperation with the Geological Survey of Canada, collected three 130-km-long refraction/wide-angle reflection profiles in the YTT and across its southern and northwestern boundaries. We present the results from the central profile, referred to as the Fairbanks South deployment, which begins approximately 30 km southeast of Delta Junction along the Alaska Highway and extends to approximately 30 km southeast of Fairbanks subparallel to the Richardson Highway (Figure 1). The velocity model from this study indicates the crust beneath the YTT averages 30 km thick with an average velocity of 6.1 km/s. The crustal velocity model has several distinguishing characteristics: (1) Crustal velocities remain

Paper number 91JB02881.
0148-0227/92/91JB-02881$05.00

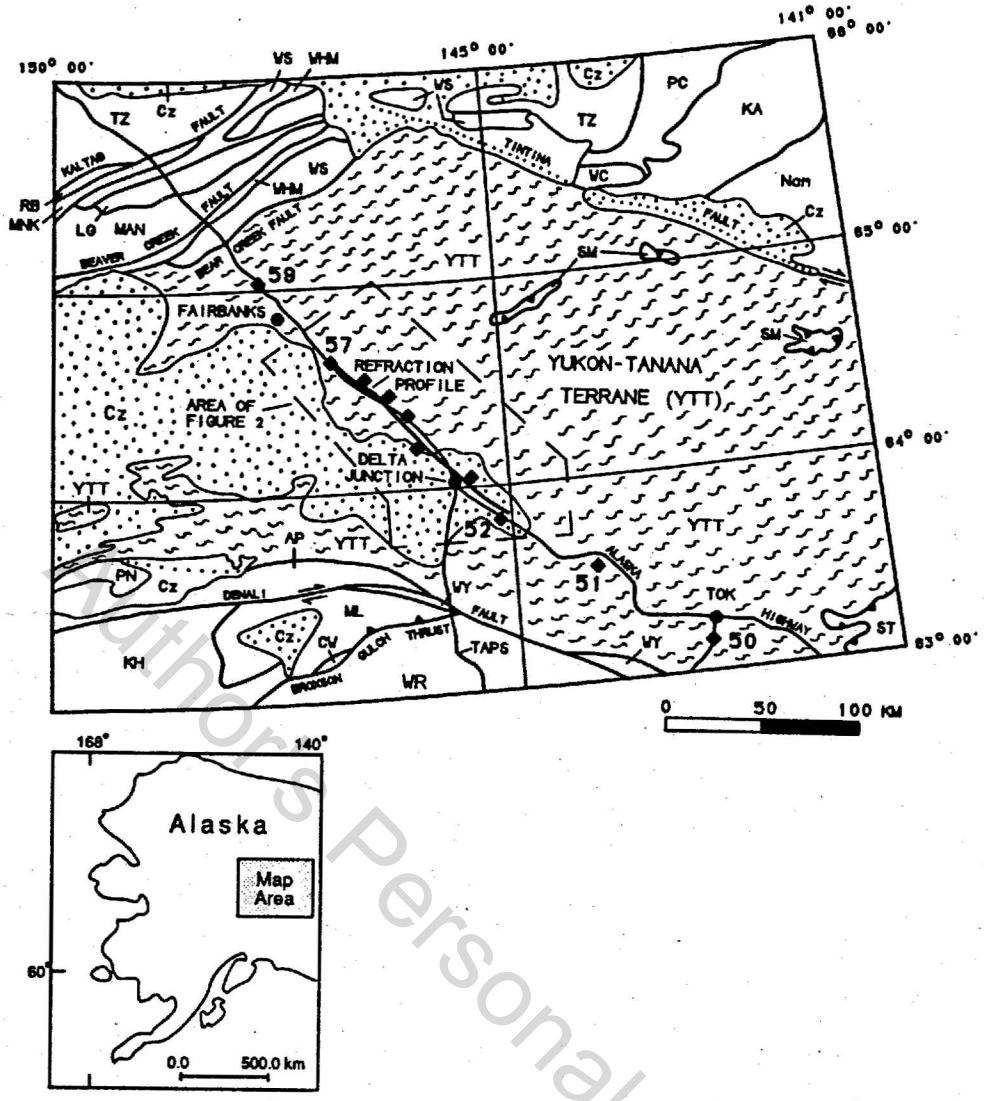

Fig. 1. Generalized tectonostratigraphic map of east central Alaska showing the location of the Yukon-Tanana and adjacent terranes. Adapted from *Foster et al.* [1987], *Jones et al.* [1987], and *Nokleberg et al.* [1989]. The Fairbanks South refraction profile is denoted by the heavy line. Shot points are designated by squares. The off-end and endpoint shots are numbered. Abbreviations are AP, Aurora Peak terrane; Cz, Cenozoic sedimentary and volcanic rocks; CW, Clearwater terrane; KA, Kandik River terrane; KH, Kahiltna terrane; LG, Livengood terrane; MAN, Manley terrane; ML, Maclaren terrane; MNK, Minook terrane; Nam, North America miogeosyncline; PC, Porcupine terrane; PN, Pingston terrane; RB, Ruby terrane; SM, Seventymile terrane; ST, Stikinia terrane; TZ, Tozitna terrane; WC, Woodchopper Canyon; WHM, White Mountains terrane; WR, Wrangellia terrane; WS, Wickersham terrane; WY, Windy terrane; YTT, Yukon-Tanana terrane.

low (≤6.4 km/s) to a depth of approximately 27 km. (2) The crust has a low average Poisson's ratio of 0.23 to approximately 27 km in depth. (3) The middle to lower crust is reflective. (4) The base of the crust consists of a thin, 3- to 5-km-thick, layer with an average velocity of 7.0 km/s overlying an upper mantle with a velocity of 8.2 km/s. The low Poisson's ratio and the low average velocity suggest that the bulk of the crust beneath the YTT has a silicic composition.

To date, most tectonic models for the YTT have focused on its origin and relation to the North American plate with only general comments on the deep crustal structure and composition. *Foster and Keith* [1974] postulated that the terrane is a continental fragment rafted into Paleozoic North America on oceanic crust. *Tempelman-Kluit* [1976] interpreted the YTT as a subduction assemblage emplaced on autochthonous North American basement. Several authors have proposed that the YTT is the remnant of a magmatic arc constructed on continental crust [*Dusel-Bacon and Aleinikoff*, 1985; *Mortensen and Jilson*, 1985]. Most recently, *Stanley et al.* [1990] proposed that the YTT is a remnant magmatic arc, with a present-day thickness of less than 10 km, suprajacent to tectonically underplated basin sediments of at least 10 km in thickness.

The Fairbanks South deployment refraction profile is the first detailed crustal study of the YTT in central Alaska and will help elucidate the nature of the crust beneath the YTT. Along with these seismic refraction results, this study incor-

porates available bedrock geologic and other geophysical data to constrain an accretionary model for the YTT. By so doing, we hope to better understand the processes which affected the current structure, composition, and evolution of the YTT and which are responsible for continental growth in general.

GEOLOGIC SETTING

Regional Setting

The southern and central parts of the YTT crossed by the refraction survey (Figure 1) are interpreted as a fragment of metamorphosed middle Paleozoic continental margin arc and older rocks [*Nokleberg and Aleinikoff*, 1985; *Foster et al.*, 1987; *Nokleberg et al.*, 1989]. The YTT occurs discontinuously in four widely separated areas of the North American Cordillera, in east central Alaska, southeastern Alaska, western Yukon Territory, and southern British Columbia [*Foster et al.*, 1987; *Jones et al.*, 1987; *Monger and Berg*, 1987; *Gehrels et al.*, 1990]. Bounding the YTT on the southwest and northeast are the dextral-slip Denali and Tintina faults respectively (Figure 1). The Denali fault has offset terranes along the southwest border of the YTT by 400 km since the mid-Cretaceous [*Nokleberg et al.*, 1985; *Plafker et al.*, 1989*b*], of which 1 to 6.5 km occurred in the Quaternary [*Stout et al.*, 1973]. The Tintina fault has offset the northwest boundary of the YTT by 450 km chiefly in the Cenozoic [*Mortensen and Jilson*, 1985]. A series of conjugate sinistral-slip faults, including the Shaw Creek fault, postdates the early Tertiary plutons in the YTT.

The YTT is one of several tectonic fragments of diverse origins that compose a collage of accreted terranes in east central and southern Alaska (Figure 1). Juxtaposed across the Denali fault are the Kahiltna, Maclaren, Windy, and Wrangellia terranes to the south with the YTT to the north. The major terranes north of the YTT are the Kandik River, Manley, Tozitna, Ruby, White Mountains, and Wickersham terranes and a part of the North American miogeocline (Figure 1) [*Churkin et al.*, 1982; *Jones et al.*, 1987; *Patton et al.*, 1989*a*, *b*]. Structurally overlying parts of the YTT are the Seventymile and Stikinia terranes (Figure 1). The Seventymile terrane occurs in a series of discontinuous klippen of obducted oceanic lithosphere of late Paleozoic and early Mesozoic age [*Foster et al.*, 1987; *Nokleberg et al.*, 1989]. The Stikinia terrane is a fragment of a Jurassic batholithic arc and older, moderate-grade metasedimentary wall rocks [*Foster et al.*, 1987; *Jones et al.*, 1987].

Southern Yukon-Tanana Terrane

Along the TACT transect, the southern YTT (Figure 2) consists mainly of a highly deformed and regionally metamorphosed sequence of Devonian metasedimentary and metavolcanic rocks and Devonian and Mississippian metagranitic rocks [*Aleinikoff and Nokleberg*, 1985; *Nokleberg and Aleinikoff*, 1985; *Foster et al.*, 1987; *Jones et al.*, 1987; *Nokleberg et al.*, 1989]. Sparse granitic plutons of mid-Cretaceous, Late Cretaceous, and early Tertiary age intrude the southern YTT (Figure 2). The southern YTT is divided into several fault bounded subterranes with shallow level metavolcanic and metasedimentary rocks occurring to the south and deeper level metagranitic and metasedimentary rocks occurring to the north (Figure 2). The subterranes along the southern part of the seismic survey are, from south to north, the Jarvis Creek Glacier, Lake George, and Butte subterranes (Figure 2). The Jarvis Creek Glacier subterrane, with locally abundant Devonian metavolcanic rocks, forms one of the structurally highest parts of the YTT. The Lake George subterrane, with locally abundant Devonian metagranitic plutons, forms the most complex bedrock unit of the YTT and is the structurally deepest level unit. The Butte subterrane, with locally abundant Devonian metavolcanic rocks, forms a major, upper level, east-northeast trending thrust sheet [*Weber et al.*, 1978; *Foster et al.*, 1987; *Nokleberg et al.*, 1989]. The Butte subterrane is correlated with the very similar Devonian metavolcanic member of the Jarvis Creek Glacier subterrane to the south and with the similar, but less metamorphosed, Devonian and Mississippian Totatlanika Schist to the west [*Foster et al.*, 1987; *Nokleberg et al.*, 1989].

The Butte subterrane displays complex structural relations. It structurally overlies the Lake George subterrane to the south and the Birch Hill and Chena River subterranes to the north (Figure 2). In turn, the Butte subterrane is structurally overlain by the oceanic lithosphere of the Seventymile terrane. At the base of the Butte subterrane is an intense zone of mylonite and mylonitic schist which displays east-southeast directed, extensional lineations [*Pavlis et al.*, 1988]. The zone of mylonites and most of the faults between subterranes are interpreted as the result of extension that occurred subsequent to prograde metamorphism of the YTT [*Pavlis et al.*, 1988; *Nokleberg et al.*, 1989].

The southern YTT is multiply deformed and metamorphosed. Each subterrane displays a unique metamorphic grade [*Nokleberg et al.*, 1989]. The Jarvis Creek Glacier and Butte subterranes display a diagnostic lower greenschist metamorphic assemblage. The Lake George subterrane exhibits upper amphibolite facies metamorphism in the structurally lower sillimanite gneiss unit. The structurally overlying pelitic schist unit exhibits lower amphibolite facies metamorphism. Retrograde metamorphism and associated penetrative deformation occur along the southern margin of the Jarvis Creek Glacier subterrane. From south to north along the Richardson Highway, lower greenschist facies metamorphic minerals systematically replace lower amphibolite facies minerals along an intense mylonitic schistosity.

Northern Yukon-Tanana Terrane

The northern YTT consists mainly of two highly deformed and regionally metamorphosed sequences (Figure 2) [*Weber et al.*, 1978; *Foster et al.*, 1987; *Nokleberg et al.*, 1989]: (1) the structurally suprajacent Birch Hill, Chena River, and Chatanika subterranes that consist of early Paleozoic(?) and Late Proterozoic and older metasedimentary rocks; and (2) the structurally subjacent Fairbanks subterrane that consists of Devonian and older metasedimentary rocks that contain lenses of metavolcanic and related rocks and locally abundant Devonian metagranitic rocks. Sparse granitic plutons of Late Cretaceous and/or early Tertiary age intrude the northern YTT (Figure 2).

The Birch Hill, Chena River, and Chatanika subterranes consist mainly of regionally metamorphosed and penetratively deformed metasedimentary rocks derived from marl, fine-grained quartz- and clay-rich sedimentary rocks, locally carbonaceous, and limestone. The Chena River subterrane is

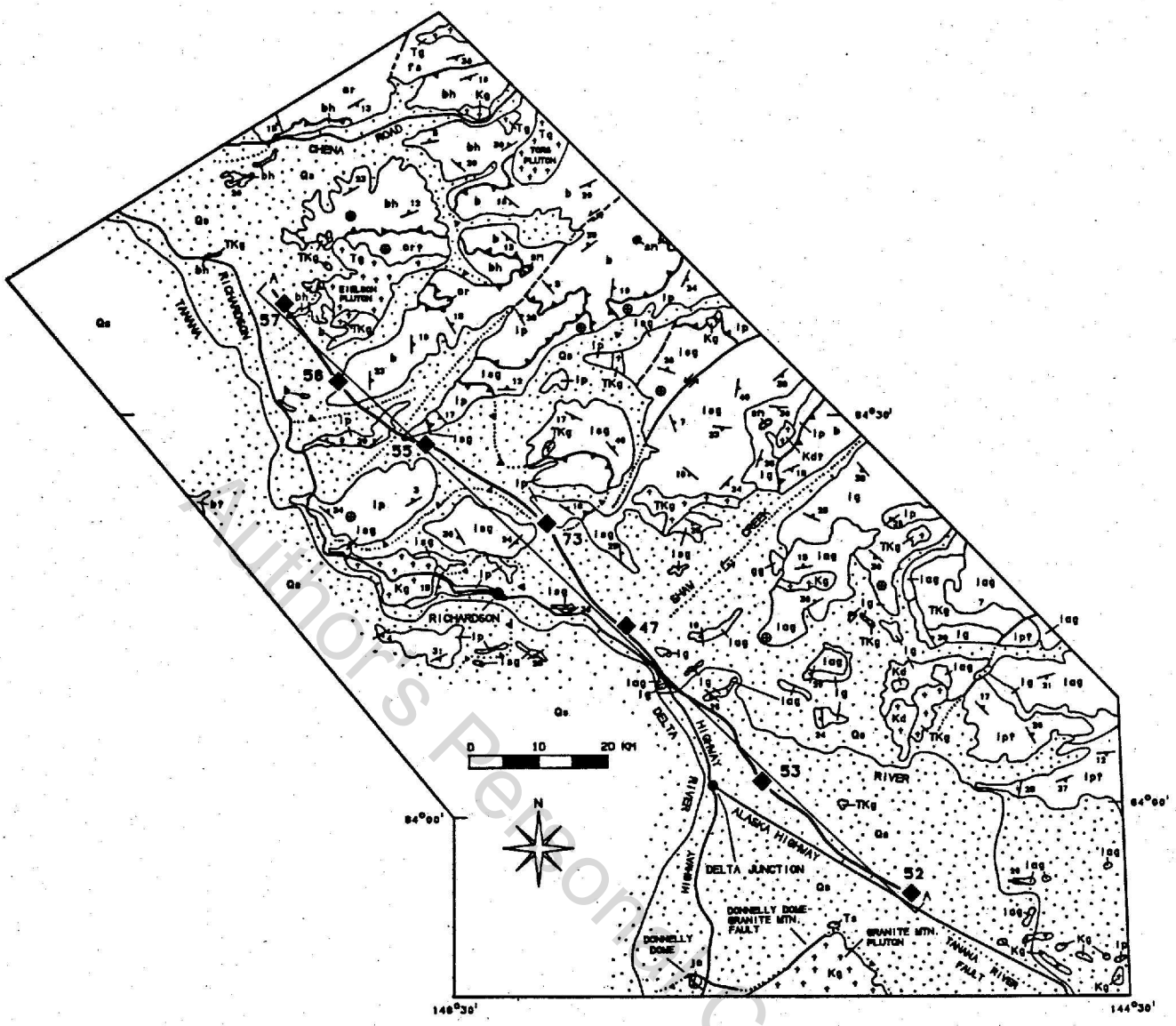

Fig. 2*a*. Generalized bedrock geologic map for the southern part of the southern Yukon-Tanana Upland, east central Alaska. Geology after *Weber et al.* [1978], *Foster et al.* [1987], and *Nokleberg et al.* [1989].

locally intruded by Devonian augen gneiss plutons and locally is in part Late Proterozoic or older where intruded by a Late Proterozoic orthoaugen gneiss [*Nokleberg et al.*, 1989]. The Birch Hill subterrane is weakly metamorphosed at lower greenschist facies and structurally overlies the Chena River subterrane which is metamorphosed up to upper amphibolite facies. Both units structurally overlie the Fairbanks subterrane. To the north, the eclogite facies and similar protolith Chatanika subterrane also structurally overlies the Fairbanks unit and is interpreted as the basal part of the metasedimentary sequence of the Birch Hill, Chena River, and Chatanika subterranes. The Fairbanks subterrane is the structurally lowest unit in the northern YTT (Figure 2), and is correlated with the very similar metasedimentary rock member of the Jarvis Creek Glacier subterrane to the south. The Fairbanks subterrane is metamorphosed up to upper greenschist facies [*Foster et al.*, 1987].

Penetrative Structures of the Yukon-Tanana Terrane

An intense penetrative mylonitic schistosity and parallel, sheared isoclinal folds form the major structure in the YTT. Generally, schistosity, axial planes of isoclinal folds, and parallel compositional layering are subhorizontal or dip gently north or south (Figure 2). Mylonitic schistosity and compositional layering are locally refolded, indicating a complex structural history. Isotopic studies indicate mainly an intense early to mid-Cretaceous age of prograde regional metamorphism and associated penetrative deformation [*Nokleberg et al.*, 1986, 1989]. The zone of retrogressive mylonites at the base of the Butte subterrane formed after the prograde event and before crosscutting of faults between subterranes by undeformed, early Tertiary granitic plutons (Figure 2). To the south, compositional layering and schistosity are warped to progressively steeper attitudes toward

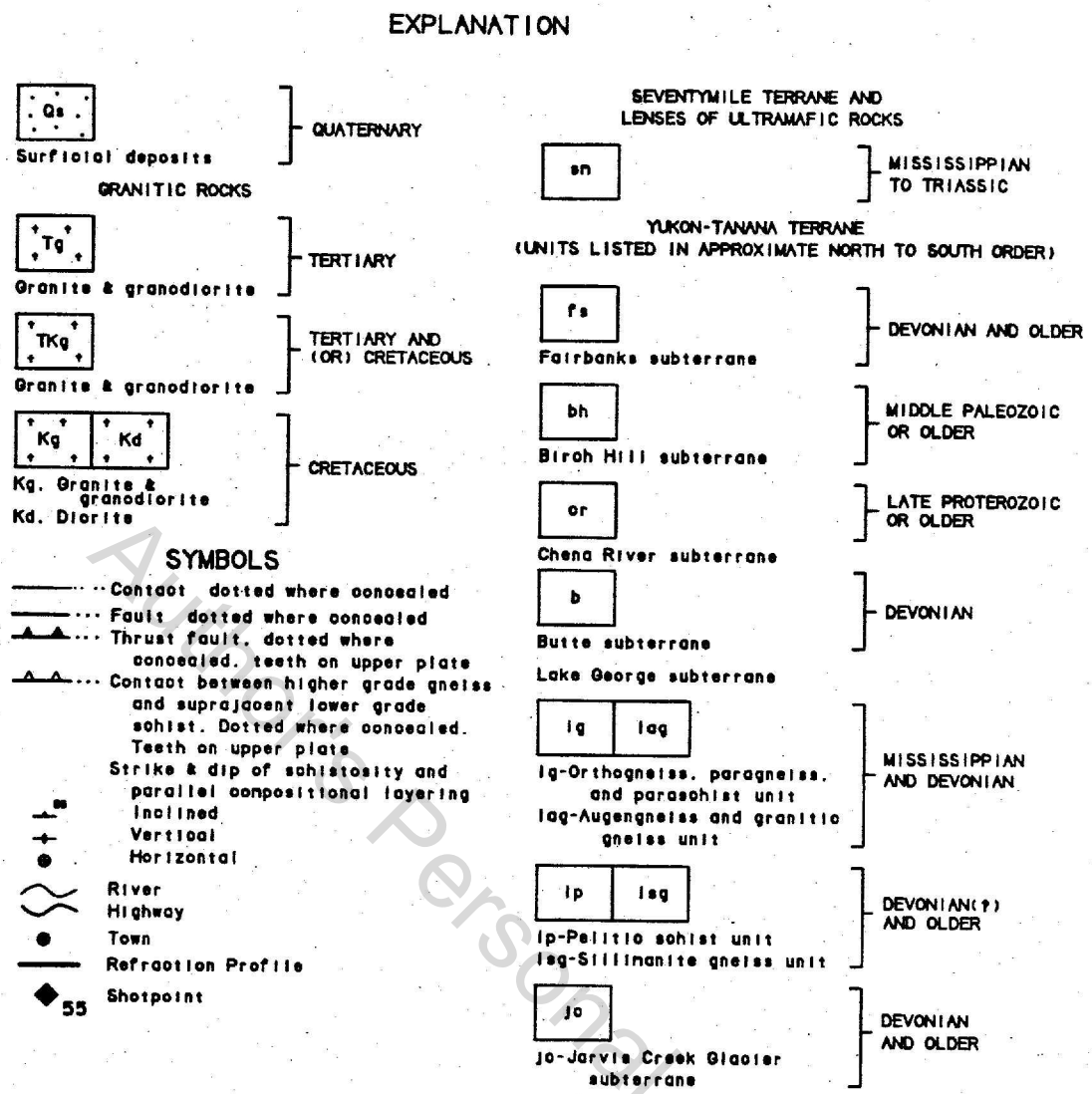

Fig. 2*b*. Explanation for Figure 2*a*.

the Denali fault, thereby forming a major regional antiform of Cenozoic age [*Nokleberg et al.*, 1989].

Faults Between Subterranes

The gently dipping, nearly concordant faults between the YTT subterranes are the loci of coincidental changes in metamorphic grade and protolith. In both the southern and northern YTT, generally lower-grade and more shallow level facies units occur over higher-grade and deeper level facies units. These relations clearly indicate that the nearly concordant faults (1) formed mainly after prograde metamorphism and (2) are mainly extensional [*Pavlis et al.*, 1988; *Nokleberg et al.*, 1989].

PREVIOUS STUDIES

Prior to the initiation of the TACT project, only a few geophysical studies of the YTT had been published. *Hanson et al.* [1968] collected a 217-km, northeast striking, seismic refraction/wide-angle reflection line centered on the Tanana Basin southwest of Fairbanks (Figure 1). Using these refraction data, together with Bouguer gravity, they modeled a crust varying in thickness from 48 km under the Alaska Range to 32 km beneath Fairbanks. This velocity model showed a simple four-layer structure with velocities of 3.7, 5.4, 5.8, and 6.4 km/s and an average crustal Poisson's ratio of 0.24. A velocity model based on quarry blasts and earthquakes from central Alaska was published by *Gedney et al.* [1980]. The crust in this model consists of two layers, a 24-km-thick 5.9 km/s velocity layer underlain by a 16-km-thick 7.4 km/s velocity layer; the total crustal thickness is 40 km, and the upper mantle is modeled with a velocity of 7.9 km/s. Earthquake swarms located near Fairbanks between 1970 and 1979 show maximum focal depths of 20 km and dominantly right-lateral focal mechanisms on NW-SE striking faults [*Gedney et al.*, 1980].

Recent geologic and geophysical studies suggest that the YTT is a thin-skinned (≤ 10 km thick) terrane. Geological mapping [*Nokleberg and Aleinikoff*, 1985; *Foster et al.*, 1987] and recent modeling of magnetotelluric and seismic reflection data [*Labson et al.*, 1988; *Stanley et al.*, 1990] suggest that the base of the southern Yukon-Tanana terrane

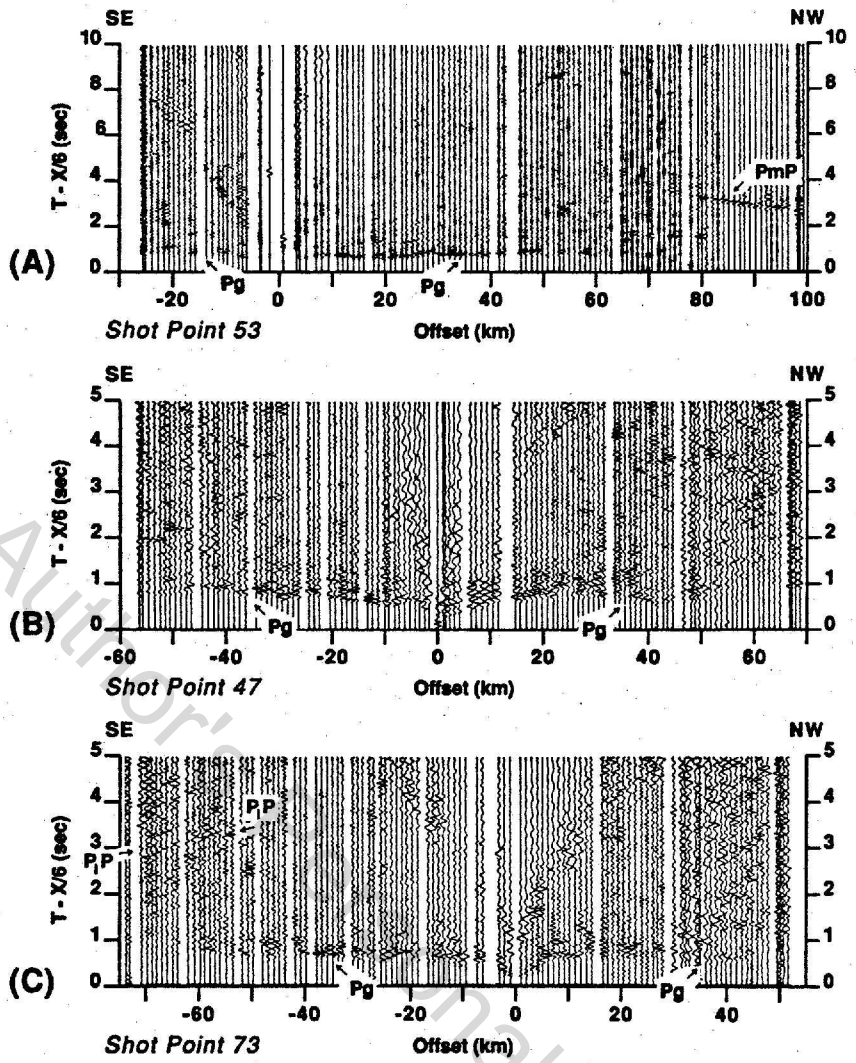

Fig. 3. Trace-normalized record sections for the shot profiles not discussed in detail. Phases labeled are *Pg*, crustal refraction; P_iP, lower crustal reflection; *Pn*, upper mantle refraction; *PmP*, Moho reflection. The record sections are plotted with a reduction velocity of 6.0 km/s except for Figure 3*i* and 3*h* which are plotted with a reduction velocity of 8.0 km/s. Note that in Figure 3*f*, *PmP* arrives before P_iP due to the crossing of these phases at far offsets.

is as shallow as 5–7 km. Additionally, the magnetotelluric studies indicate a low resistivity (2–10 ohm m) layer beneath the YTT extending from about 10 km to about 20 km in depth. This highly conductive, midcrustal to lower-crustal layer is interpreted as graphite-rich, underplated Mesozoic flysch thrust under the southern margin of the Yukon-Tanana terrane along an ancestral branch of the Denali fault [*Stanley et al.*, 1990]. Recent studies by *Gehrels et al.* [1990] suggest that most of the (former) Tracy Arm and eastern Taku terranes in southeastern Alaska can be correlated with the YTT and that this major fragment of the YTT is thrust over Mesozoic flysch of the Gravina-Nutzotin belt and the Wrangellia terrane.

In addition to the studies mentioned above, heat flow, gravity, and aeromagnetic surveys have been conducted in the YTT. Heat flow measurements taken from two holes in the vicinity of Fairbanks and two holes near the Alaska-Canada border ranged from 75 to 1000 mW/m^2 [*Lawver et al.*, 1981]. Gravity measurements along the Fairbanks South deployment show a 60-mGal decrease from northwest to southeast, which is correlated with a crustal thickening toward the Alaska range [*Woollard et al.*, 1960; *Barnes*, 1977]. Magnetic anomalies in this region are related to lithologic and metamorphic contacts. The Shaw Creek fault (Figure 2) is well defined as a linear interruption of magnetic anomalies on the aeromagnetic map [*Griscom*, 1978].

DATA COLLECTION

The Fairbanks South deployment consisted of 130 km of reversed seismic refraction/ wide-angle reflection data (Figures 1 and 2). Instruments spaced 1 km apart recorded 11 shots varying in size from 227 to 2724 kg of explosive. Shots were detonated in 50-m-deep drill holes or shallow (3–15) glacial lakes. Shot points are spaced between 15- and 30-km in-line and at 75-km intervals off-end affording a maximum offset of 280 km. The in-line shots provide velocity control on the upper 5–10 km of crust within the spread. The off-end shots provide reversed sampling of the crust to Moho depths. The recording instruments consisted of 120 U.S. Geological Survey cassette recorders [*Healy et al.*, 1982; *Murphy*, 1988] and 12 Geological Survey of Canada (GSC)

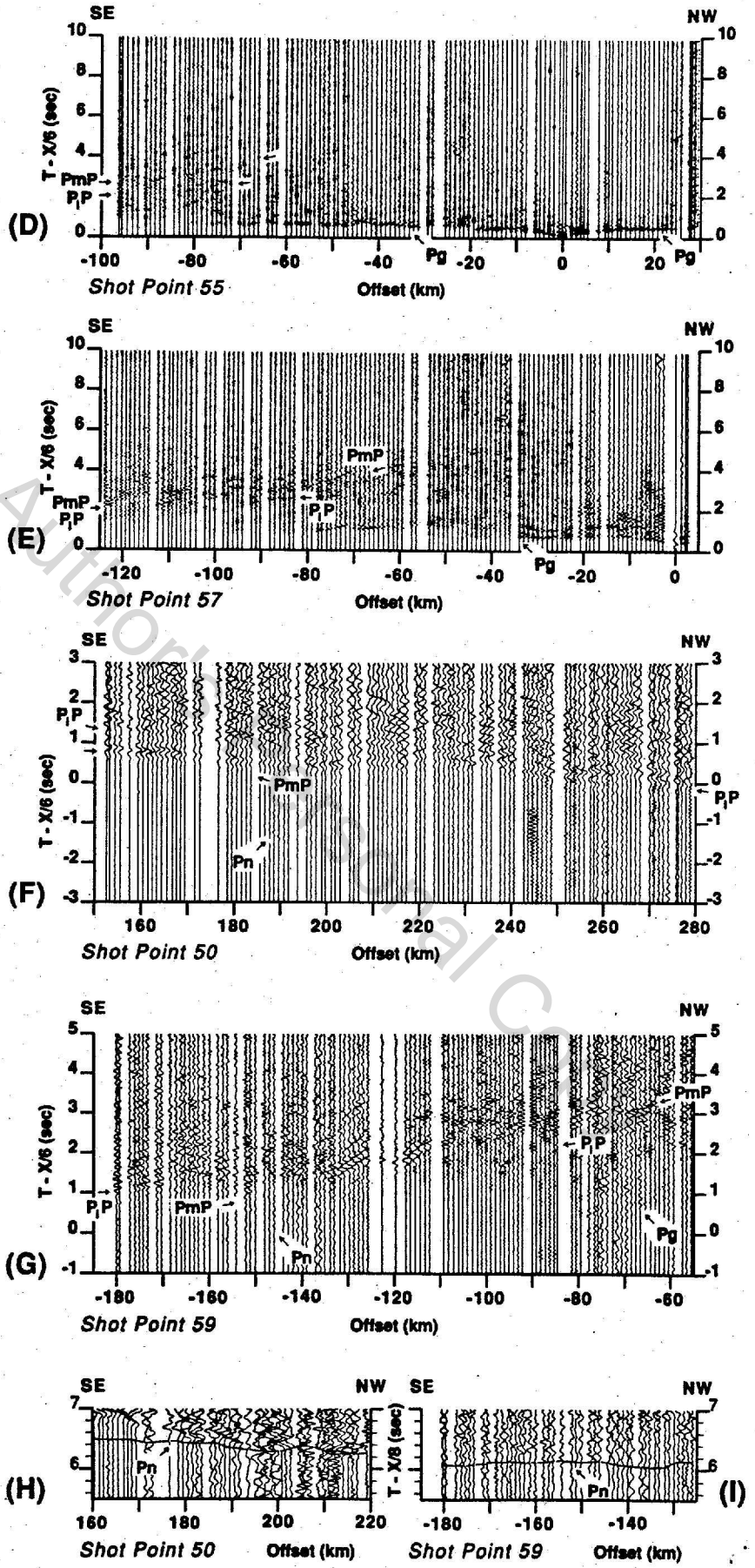

Fig. 3. (continued)

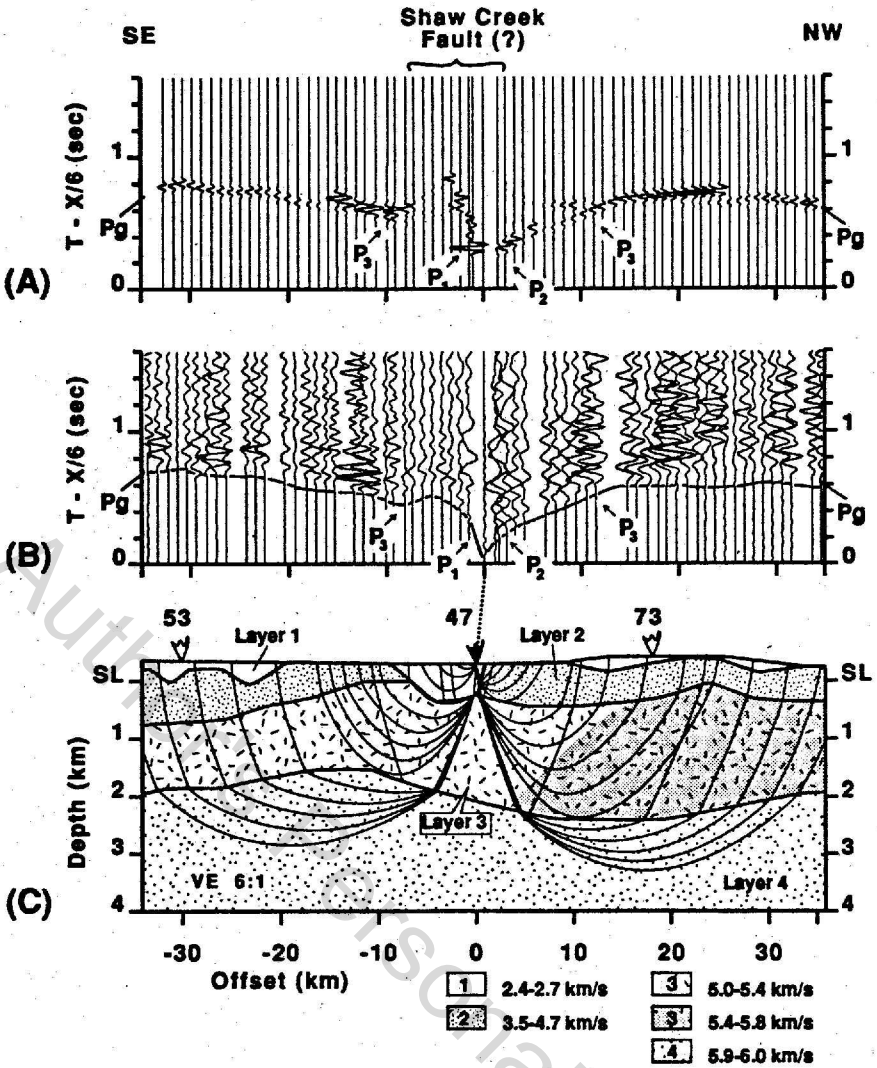

Fig. 4. A ray diagram for shot point 47 which straddles the projection of the Shaw Creek fault. (*a*) Ray theory synthetic. (*b*) Data with calculated travel time curves overlain. (*c*) Ray diagram. Both the data and synthetic are plotted with a reduction velocity of 6.0 km/s and in true amplitude format. True amplitude format includes corrections for instrument gain, shot-receiver offset, and shot efficiency [see *Beaudoin et al.*, 1989]. Crustal phases are labeled P_1, P_2, P_3, and Pg.

PRS-1 digital recorders; both systems utilized 2-Hz vertical component geophones. The USGS instruments record an FM multiplexed analog signal on magnetic tape. This analog signal was converted to digital format using a sampling interval of 5 ms. The GSC instruments record a digital signal sampled at 8 ms. For a more detailed account of the data processing and the merging of the USGS cassette recorder data with the GSC digital recorder data, see *Beaudoin et al.* [1989].

The instruments were deployed at presurveyed sites that were located using orthophoto quadrangles, aerial photographs, and topographic maps, all at a scale of 1: 63,360. Site locations have estimated errors of 50 m laterally and 10 m in elevation. Seismic traces have timing accuracies of about 20-30 ms, given instrument clock drifts and some uncertainty in matching GSC and USGS digital seismic traces [*Beaudoin et al.*, 1989].

DATA CHARACTERISTICS

Major compressional wave phase characteristics of the Fairbanks South deployment are shown in Figure 3. Although all of the recorded shots were used in the modeling, only several shot points which exemplify the characteristics are discussed in detail below (Figures 4–7). Additional information is provided by wide-angle shear wave reflections from the lower crust (S_lS) (Figure 11) and will be discussed following the compressional wave sections. In the discussion that follows, upper crust refers to depths of <8 km, middle crust refers to depths of 8–20 km, and lower crust refers to depths ranging from 20 km to Moho.

Compressional Wave Data

Upper crust. Near-surface phases ("P_1") exhibit high amplitudes and variable velocities. These velocities and

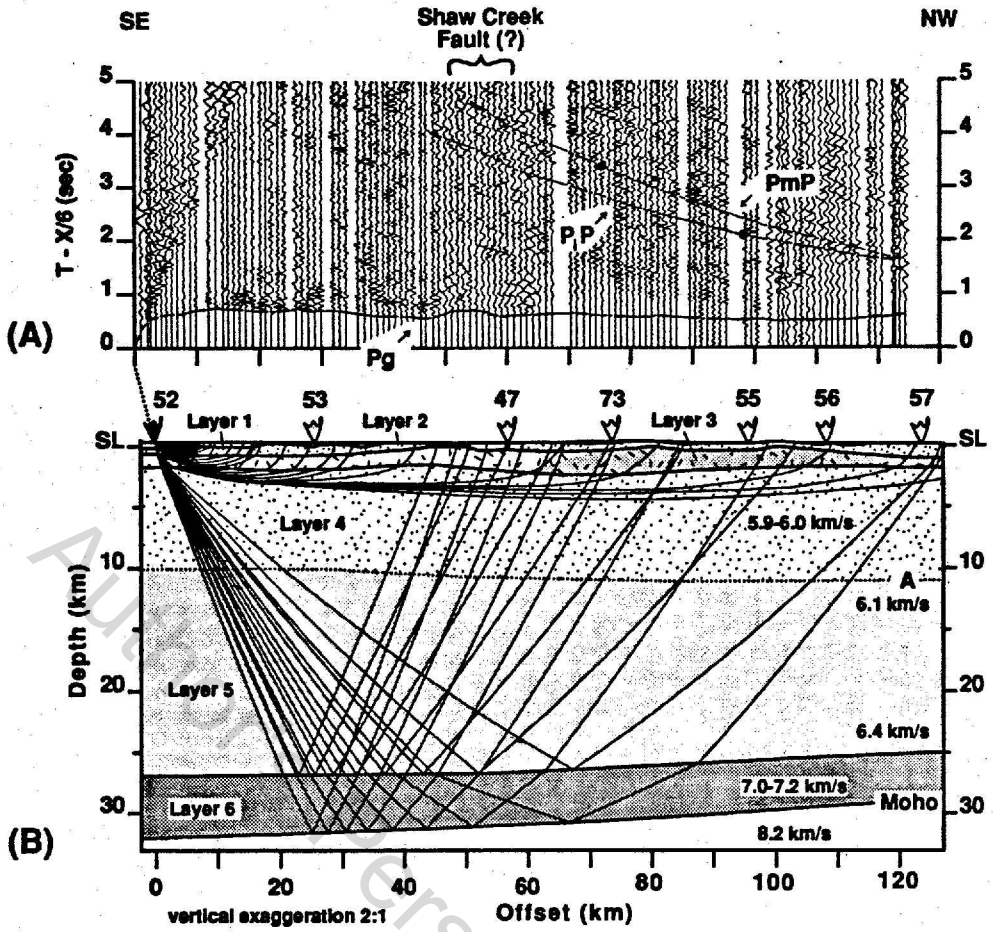

Fig. 5. A ray diagram for shot point 52. (*a*) Data with calculated travel time curves overlain. (*b*) Ray diagram. The data plotted in trace normalized format with a reduction velocity of 6.0 km/s. Phases labeled are *Pg*, crustal refraction; P_iP, lower crustal reflection; *PmP*, Moho reflection. For both P_iP and *PmP* the critical point is denoted by a solid dot.

corresponding velocity gradients are poorly constrained due to the 1-km spatial sampling along the profile; near-surface phases were sampled by two seismometers at best before crossover by later arrivals. Following these near-surface arrivals, three upper crustal phases are recognized (labeled "P_2", "P_3" and "*Pg*"; Figure 4). These phases have average apparent velocities of 4.2, 5.4, and 6.0 km/s, respectively. The most pronounced upper crustal arrival is a laterally continuous *Pg* phase with an average apparent velocity of 6.0 km/s; this phase is observed from about 10 to 130 km (Figures 5*a* and 6*a*). *Pg* has very little travel time relief (≤ 0.08 s on average) across the entire profile, with the exception of a region near the Shaw Creek fault, suggesting little complexity in the velocity structure of the upper crust along this profile. The 0.2-s delay in *Pg* near the Shaw Creek fault (Figures 5 and 6) is a smooth bump in the travel time curve seen on the same stations for all shots and indicates a broad zone of low-velocity material as opposed to an abrupt vertical contact. This near-surface velocity variation observed near the Shaw Creek fault is shallow as evidenced by the onset of *Pg* in both directions at about 12 km offset (Figure 4*b*). *Pg* amplitudes are largest in the range of 5–45 km in offset, beyond which they decrease (Figures 5*a* and 6*a*). The weaker amplitude beyond 45 km suggests a decreasing velocity gradient at about 5 km in depth [*Banda et al.*, 1982].

Middle to lower crust. An increase in energy return from middle to lower crustal levels, relative to upper crustal energy, is observed in these data beginning at approximately 30 km in offset from 1 to 4 s reduced time (Figures 3, 5, and 6). Reflections from the middle to lower crust are not laterally coherent (typically ≤ 8 km in lateral extent) and suggest discontinuous laminations or an increase in scattering at these levels. Arriving from the base of this reflective sequence is a distinct, lower crustal reflection (labeled "P_iP"; Figures 3 and 5–7) on several of the in-line shot profiles and on all of the off-end shot profiles. The identification of P_iP is based primarily on the amplitudes at offsets of greater than 140 km (Figures 3*f*, 3*g*, and 7). The reflection P_iP extends to offsets of 280 km (Figure 3*f*) where it has asymptotic velocities of 6.3–6.5 km/s. The persistence of P_iP energy to large offsets indicates a low-velocity gradient in the lower crust (Figures 3*f*, 3*g*, and 7); a high-velocity gradient would focus the P_iP reflection to a smaller range of offsets than is observed. Additionally, the asymptotic velocity observed for P_iP at far offsets indicates that lower crustal velocities directly above this layer do not exceed 6.5 km/s. The Moho reflection (*PmP*) varies in character from a largely unicyclic, well defined phase (Figures 3*a* and 6*a*) to a multicyclic, poorly defined arrival (Figures 3*d*, 3*e*, and 5*a*). This variable character implies the structure of the Moho transition is laterally heterogeneous beneath our pro-

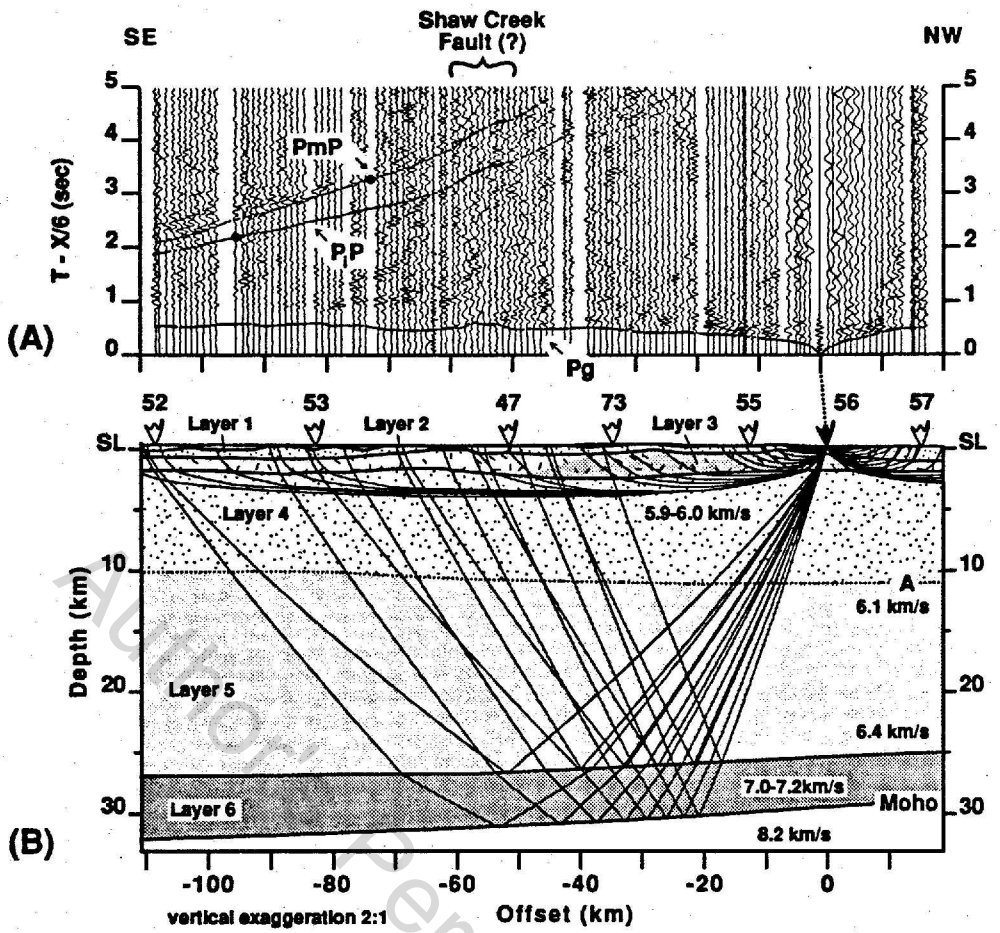

Fig. 6. A ray diagram for shot point 56. (*a*) Data with calculated travel time curves overlain. (*b*) Ray diagram. The data are plotted in trace normalized format with a reduction velocity of 6.0 km/s. Phases labeled are *Pg*, crustal refraction; P_iP, lower crustal reflection; *PmP*, Moho reflection. For both P_iP and *PmP* the critical point is denoted by a solid dot.

file. A low velocity gradient in the upper mantle is inferred from a weak and emergent Moho refraction (Pn) (Figures 3*f* to 3*i*, and 7*a*).

Shear Wave Data

Wide-angle intracrustal shear wave reflections are not discernable in these data. The near-surface shear wave reflections, if present, are most likely masked by the surface wave. Middle to lower crustal reflectivity is discontinuous for compressional waves, indicating that the crustal reflection character for shear waves might also be discontinuous. Additionally, several studies have demonstrated that lower crustal lamellae that are reflective for *P* waves can be relatively transparent for *S* waves at wide angles [*Wenzel et al.*, 1987; *Holbrook et al.*, 1988]. A prominent S_iS, a full path shear wave reflection from the lower crust, is evident on several of the record sections (Figure 11). Like its compressional wave counterpart, S_iS is laterally extensive. Additionally, P_iS, a *P* to *S* wave phase converted in the lower crust, is present in these data (Figure 10). These two phases, S_iS and P_iS, will be used to further constrain estimates of the bulk crustal composition beneath the Fairbanks South deployment.

VELOCITY MODELS

Compressional Wave Model

A compressional wave velocity model (Figures 4–7 and 8*b*) was constructed by forward modeling the travel time and amplitude information. One-dimensional slope intercept modeling of record sections from all shot points provided a basis for constructing a two-dimensional velocity model. Iterative perturbations of this two-dimensional model, using asymptotic ray theory [*Červený et al.*, 1977; *Luetgert*, 1988] to fit travel times, further determine the crustal velocity structure. These iterations continued until the calculated travel times fitted the data to within an average of ±0.05 s. Finally, both ray theory synthetics [*McMechan and Mooney*, 1980; *Luetgert*, 1988] and reflectivity synthetics [*Fuchs and Müller*, 1971] were used to model the amplitude characteristics of these data.

Error estimates. In order to determine the error bounds on our velocity model, we tested the sensitivity of the travel time fit to perturbations of the velocity structure and interface positions. Unfortunately, unlike travel time inversion methods [see *Hawman et al.*, 1990; *Lutter et al.*, 1990], quantified errors are not a direct by-product of forward modeling techniques and must be determined separately.

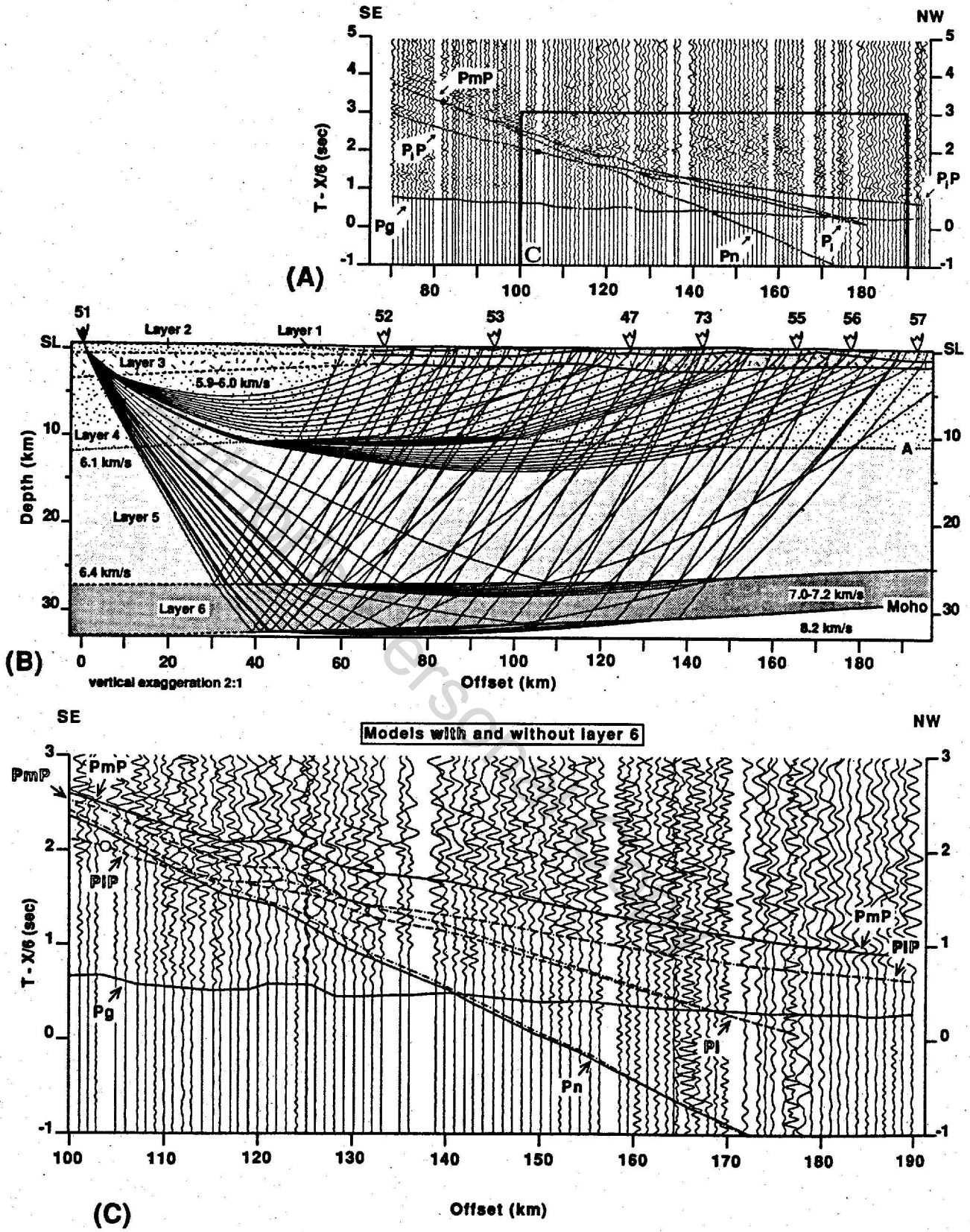

Fig. 7. A ray diagram for shot point 51. (*a*) Data with calculated travel time curves overlain. (*b*) Ray diagram. (*c*) A comparison of calculated travel time curves for models with (dash-dotted line) and without (solid line) layer 6. Significant travel time misfits occur for *PmP* with the omission of layer 6. The data are plotted in trace-normalized format with a reduction velocity of 6.0 km/s. Phases labeled are *Pg*, crustal refraction; P_i, lower crustal refraction; P_iP, lower crustal reflection; *Pn*, upper mantle refraction; *PmP*, Moho reflection. For both P_iP and *PmP* the critical point is denoted by a solid dot.

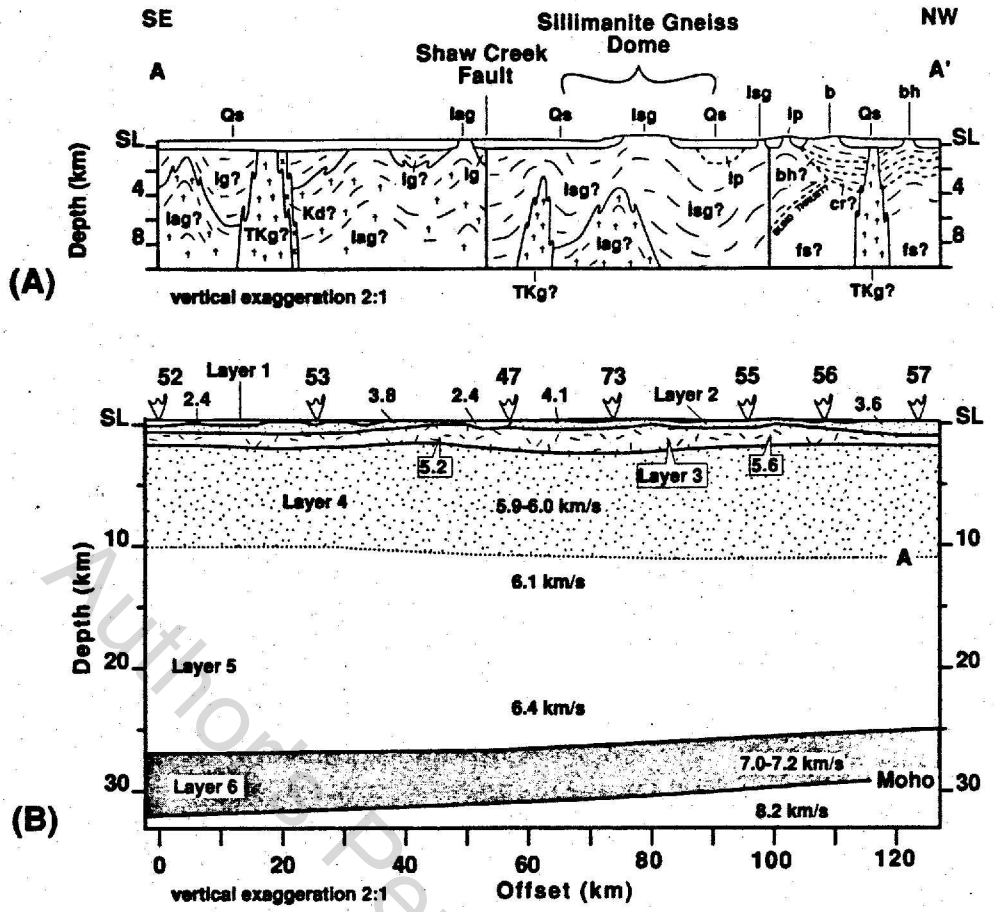

Fig. 8. A comparison between the geologic and the velocity model interpretations. The shot points are the numbered symbols. 2.4 is velocity in kilometers per second. See Figure 2 for geologic units. (*a*) Geologic cross section. (*b*) Velocity model.

For the uppermost crust (layers 1 = "P_1", 2 = "P_2", and 3 = "P_3"), travel times can be picked with an accuracy of ±0.02 s. The travel time fit for these layers is sensitive to velocity perturbations of greater than ±0.10 km/s and interface position perturbations of greater than ±100 m; significant travel time misfits (≥ 0.025 s) occur. For *Pg* (layer 4), travel times can be picked with an accuracy of ±0.02–0.05 s. The lateral extent of *Pg* makes its travel time fit very sensitive to velocity perturbations. Velocity perturbations of ±0.05 km/s produce travel time misfits of ≥ 0.10 s at large offsets (≥ 50 km). For the middle to lower crust and upper mantle (layers 5, 6, and 7), travel times can be picked with an accuracy of ±0.02–0.05 s and ±0.05–0.10 s for first breaks and secondary arrivals, respectively. For these layers the finite penetration of diving rays affords velocity control at the top of each layer but weaker control at its base (Figures 5*b*, 6*b*, and 7*b*). To avoid travel time misfits of ≥ 0.10 s for phases P_iP, P_i, *PmP*, and *Pn*, velocity errors must be less than ±0.10 km/s, ±0.20 km/s, and ±0.10 km/s for layers 5, 6, and 7 respectively. Travel time fits for P_i, P_iP, *Pn*, and *PmP* are sensitive to interface position perturbations of ±1 km. In summary, velocity errors range from ±0.05 to 0.20 km/s, and the velocity model has estimated interface depth errors on the order of a few hundred meters in the near surface to ±1 km in the lower crust.

Upper crust. The most striking feature of the upper crust beneath the Yukon-Tanana terrane is a simple seismic velocity structure (Figure 8*b*). Below the low-velocity surface layer (layer 1) with velocities of 2.4–3.0 km/s, little velocity or interface structure is required by the data. Layer 2, with velocities of 3.5 km/s at the surface to 4.7 km/s at its lower interface, extends to the surface where shots and instruments were on bedrock sites. Layer 3 is 1–2 km thick with an average velocity of 5.4 km/s. Velocity gradients for layer 1 have been assigned at 0.35 s^{-1} based on amplitude modeling of the succeeding phases; velocity gradients of >0.4 s^{-1} hindered the propagation of energy into the crust and produced insufficient energy in later crustal phases. Layers 2 and 3 have gradients ranging from 0.2 to 0.35 s^{-1} based on refraction branch curvature. These high gradients in layers 1–3 suggest that compaction and crack closure govern velocity increases within these layers [see *Birch*, 1961; *Christensen*, 1965, 1966*b*]. The division of the upper 2 km of crust into three distinct layers is warranted by the existence of travel time cusps and regions of higher amplitude at or near crossover points between velocity branches (Figure 4*b*). An attempt to model this portion of the crust with a single gradient zone did not successfully match the amplitude-range distribution of the shallow crustal branches. Gradients in excess of 1.0 s^{-1} were needed and hindered penetration of energy below this zone. Layer 4 has an average velocity of 5.9 km/s. The upper 2 km of this layer

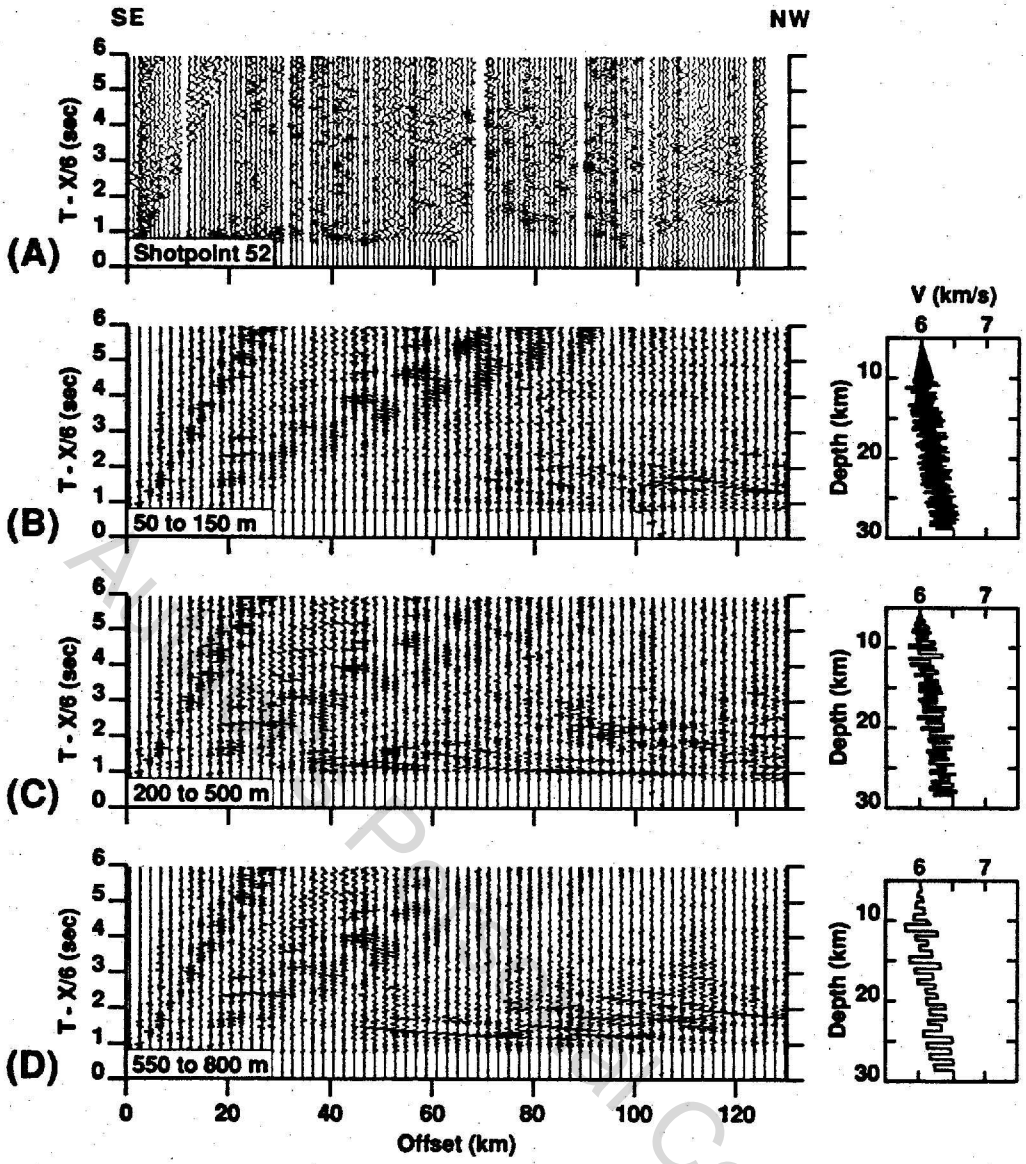

Fig. 9. Record section for shot point 52 compared to three reflectivity synthetic record sections. The record sections are plotted in trace normalized format with a reduction velocity of 6.0 km/s. The velocity function for each synthetic is displayed to the right. Layer thickness vary randomly for each model within the bounds listed on the synthetic record sections. Velocity variations between lamellae in the models are ≤ 0.5 km/s. (*a*) Data. (*b*) Layers with thickness of 50–150 m. (*c*) Layers with thickness of 200–500 m. (*d*) Layers with thickness of 550–800 m.

required a velocity gradient of 0.2 s^{-1} to focus *Pg* energy between 5 and 45 km in offset. Below this higher gradient, a velocity gradient of 0.02 s^{-1} was determined.

Two minor inhomogeneities occur in the upper crustal velocity structure. First, the region near the Shaw Creek fault exhibits both travel time and amplitude anomalies (Figure 4*b*). The smooth delay in travel time requires the modeling of this region as a 10-km-wide, 1-km-deep basinlike thickening of layer 1 as opposed to a discrete vertical boundary. Second, near the sillimanite gneiss dome [*Dusel-Bacon and Foster*, 1983] (between shot points 73 and 56), a minor velocity perturbation of 0.5 km/s occurs in the upper 2 km of the crust (layer 3 shading; Figure 8*b*) and coincides with the observed increase in metamorphic grade toward the center of the gneiss dome. Both of these velocity features are shallow, extending to ≤ 2 km in depth.

Middle and lower crust. We chose to delineate the boundary between the upper and middle crust by a single interface, ("A"; Figure 8*b*). This decision is based on the need to define a boundary approximating the top of the reflective middle to lower crust in the two-dimensional velocity model and the crustal conductivity results of *Stanley et al.* [1990]. We further constrain the position of this boundary and show it to coincide with the top of the reflective middle to lower crust using reflectivity synthetics below (Figure 9). As modeled, this interface marks a velocity increase from 6.0 km/s at the base of layer 4 to 6.1 km/s at the top of layer 5. Early models divided layer 5 into several discrete layers. However, the lack of convincing coherent reflections from this region and the minor velocity contrasts across interfaces in these models (typically 0.05 km/s) favor modeling layer 5 as a single layer. In this model, no distinct

boundary occurs between middle and lower crust. Layer 5 is extended to 26–28 km in depth where it has a velocity of 6.4 km/s. At this depth a 3- to 5-km-thick region, layer 6, with velocities of 7.0–7.2 km/s, marks the transition from lower crust to mantle. As discussed below, interface "A" roughly coincides with the subhorizontal boundary between the highly resistive rocks of the YTT at the surface and the highly conductive rocks of interpreted tectonically underplated Mesozoic flysch and other highly conductive units.

The transition from upper to middle crust and the middle to lower crustal reflectivity was modeled by one-dimensional reflectivity synthetics [*Fuchs and Müller*, 1971] (Figure 9). The lateral homogeneity of velocities in our model justifies one-dimensional modeling of a representative shot profile to characterize middle and lower crustal reflectivity beneath the seismic array. Shot point 52 was chosen to provide maximum in-line offsets. The model used the upper crustal velocity structure from the two-dimensional velocity model down to interface "A." Below this interface, lamellae thicknesses and velocities were allowed to vary randomly while keeping the average velocity of the lower crust in agreement with the two-dimensional velocity model (Figure 9). We do not suggest that these laminations are laterally continuous for tens of kilometers. Rather, our objective was to model the general energy distribution observed in these data. However, we recognize a minimum lateral extent of approximately 2.5–4 km (a half wavelength Fresnel zone) for these laminations to be imaged by our array. A model with layers ranging from 200 to 500 m (approximately 0.4 to 1 λ) (Figure 9*c*) in thickness best matches the observed energy distribution between approximately 30 and 130 km in offset and 1 and 4 s reduced time. Velocity variations between adjacent layers do not exceed ±0.5 km/s. It was necessary to introduce a velocity gradient at the top (6–10 km in depth) of this reflective sequence to avoid drastically over predicting amplitudes from midcrustal levels at offsets of 40–50 km and 1 s reduced travel time. A model with layer thicknesses of less than 200 m (Figure 9*b*) produces too little energy between offsets of 30 and 70 km but matches the data fairly well at offsets greater than 70 km; the thin layers are relatively transparent to the dominant frequency (8 Hz) of these data. A model with layer thicknesses of greater than 500 m (Figure 9*d*) also fails to produce sufficient energy for offsets of 30–60 km. In addition, reflector continuity is high in this model, indicating that if velocity anomalies in this region of the crust have thicknesses of greater than one wavelength, their lateral extent has to be limited.

Moho transition. The crust-mantle boundary is modeled at an average depth of 30 km. The transition from lower crust to mantle is modeled over a 3- to 5-km-thick zone, layer 6. A transition zone is motivated by the following data characteristics: (1) The lack of identifiable precritical *PmP* (Figures 3, 5, and 6). (2) The variable nature of *PmP* along the profile (Figures 3, 5, and 6). (3) The presence of P_iS (Figure 10). The presence of P_iS, although weak, suggests that the top boundary of this transition zone is a first-order discontinuity [*Fuchs*, 1975]. The lack of precritical *PmP* suggests that this transition zone has a finite thickness [*Braile and Chiang*, 1986]. However, a closer receiver spacing might reveal coherent precritical *PmP*. Forward modeling of P_iP and *PmP* requires a velocity of 7.0 ± 0.2 km/s for this layer (Figure 7). A gradient is used to fit the observed truncation of the *PmP* travel time curve at approximately 200 km offset. Amplitude modeling (Figure 10), using the reflectivity results for the middle and lower crust as a starting model, confirms the need for this higher gradient suggested by the travel time fit. Modeling layer 6 with no gradient produces too much energy in the forward branch of P_i and *PmP* at offsets greater than 200 km (Figure 10*b*). A gradient of 0.04 s^{-1} matches the truncation of both P_i and *PmP* at 200 km offset as observed in the data (Figure 10*c*). Modeling layer 6 with a simple gradient satisfactorily predicts *PmP* for shot profiles where *PmP* is a strong, unicyclic phase in the range of 80–100 km in offset (compare *PmP* in Figure 6*a* with Figure 10*d*). To produce the more multicyclic, poorly defined *PmP* observed for shot points 52 and 57, we tried several approaches. First, by increasing the velocity at the base of layer 6, thereby reducing the reflection coefficient across the crust-mantle boundary, we hoped to reduce the amplitude of *PmP* sufficiently to be lost in lower crustal energy. This approach still produced a strong *PmP* reflection. Second, we introduced layering in layer 6 with the same parameters used for the middle to lower crust as discussed above. This approach proved satisfactory for reproducing the multicyclic, poorly defined *PmP* observed for shot profiles 52 and 57 (compare Figure 5*a* with Figure 10*e*). It is also possible that the poorly defined *PmP* on shot points 52 and 57 is due, in part, to an increase in scattering along similar *PmP* travel paths for these reversing shot profiles.

Layer 6 produces a "hidden" arrival with a critical point at approximately 100 km making it a difficult phase to discern on the in-line shot profiles. For this reasons, early models excluded this layer. These early models were still able to match the first break and *PmP* (now interpreted at far offsets as P_iP) travel time curves to a first order (Figure 7*c*). However, both the curvature of the *PmP* reflection and the travel times of *Pn* could not be matched simultaneously. Based on the travel time mismatch for *PmP* between approximately 150 and 200 km in offset and on the prominent precritical P_iP observed for shot point 51 (between 70 and 100 km at approximately 3 s reduced time; Figure 7*a*), an additional lower crustal layer, layer 6, was introduced. The high precritical amplitudes observed for P_iP can be attributed to interference effects within the layered middle and lower crust. The introduction of layer 6 does little to change the overall velocity structure of the crust. The average crustal velocity is 0.05 km/s higher in models with layer 6 than without and the Moho is approximately 1 km deeper in models with layer 6 than without. The recognition of layer 6 in the velocity model also changes the interpretation of far offset phase correlation. The far offset arrival interpreted as *PmP* in early models is now interpreted as P_iP.

Shear Wave Model

The presence of S_iS on several of the profiles allows for the determination of an average crustal Poisson's ratio. By converting the compressional wave velocity model to shear-wave velocity models, using several values of Poisson's ratio, travel times for S_iS were calculated (Figure 11). An average crustal Poisson's ratio of 0.23 best models the onset of S_iS. We feel that this determination of Poisson's ratio is not biased either by velocity anisotropy or by misinterpretation of the S_iS phase for the following reasons. First, although anisotropy is strong and pervasive in sampled lithologies along the profile, propagation for *P* and *S* waves

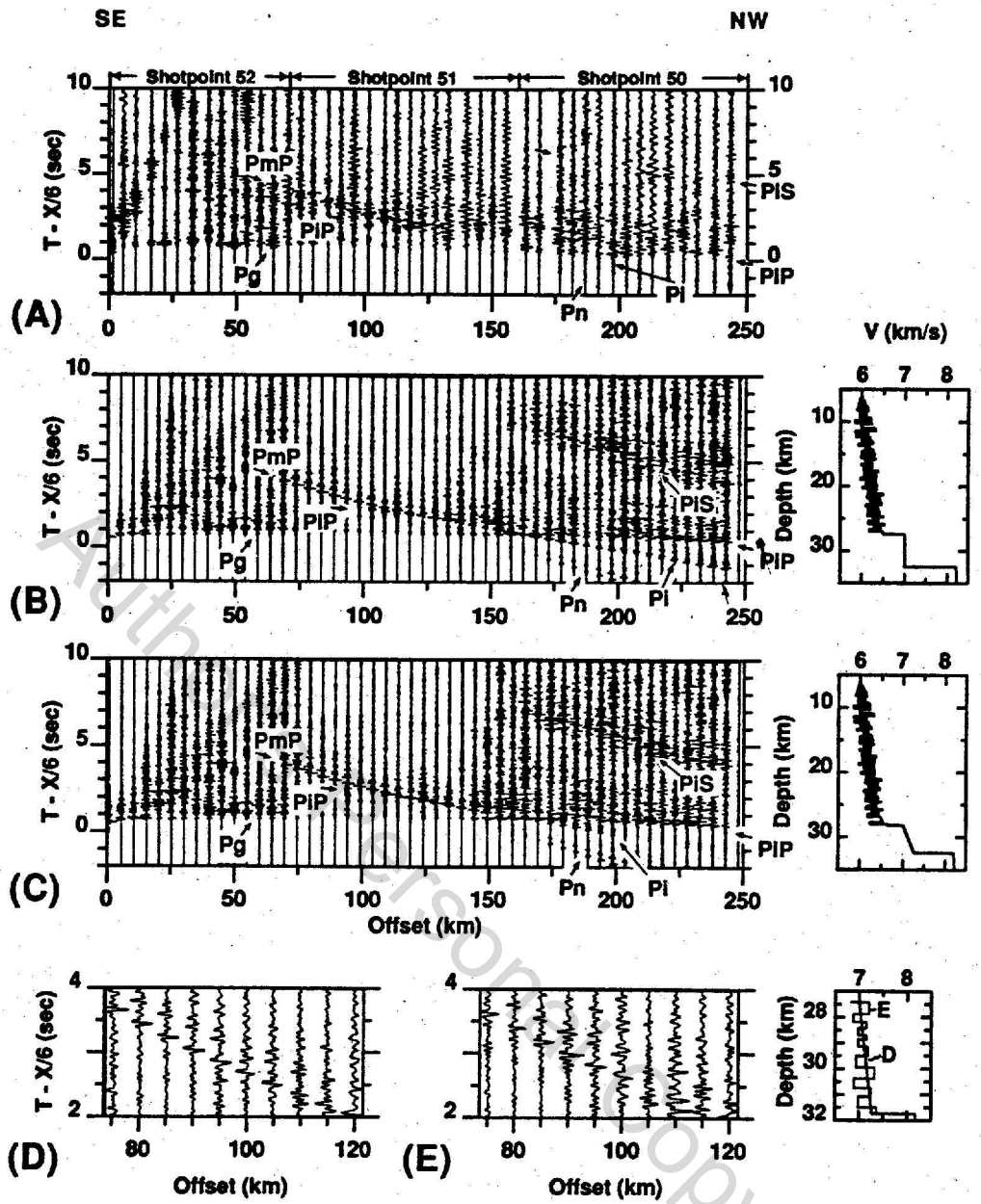

Fig. 10. A composite of shot points 50, 51, and 52 compared to reflectivity synthetics. The record sections are plotted in trace normalized format with a reduction velocity of 6.0 km/s. The data have been winnowed to a trace spacing of ~5 km for display purposes. The synthetic models constructed using the preferred laminated middle to lower crustal structure (from the model of synthetic record C; Figure 9*c*) to a depth of approximately 27 km. At this depth, a 4-km-thick lower crustal layer is introduced. The velocity function for each synthetic is displayed to the right. Phases labeled are *Pg*, crustal refraction; P_i, lower crustal refraction; P_iP, lower crustal reflection; P_iS, lower crustal converted phase; *Pn*, upper mantle refraction; *PmP*, Moho reflection. (*a*) Data. (*b*) No gradient in lower crustal layer. (*c*) A gradient of 0.04 s^{-1} in lower crustal layer. (*d*) *PmP* from synthetic with gradient, model C. (*e*) *PmP* for a lower crustal layer with 200- to 500-m-thick lamellae.

are parallel to the regional textural fabric defined by aligned micas, feldspar, quartz, and other minerals. Propagation directions parallel to this fabric is the fast direction for both compressional and shear waves [see *Christensen*, 1966*a*, *b*]. For a constant Poisson's ratio, P_iP and S_iS follow roughly the same ray path. Therefore Poisson's ratio should not be biased by the anisotropy. Second, S_iS can be distinguished from a converted arrival off a midcrustal interface (8 km depth) simply by travel time. That is, if we had inadvertently interpreted an *S* wave which converted to a *P* wave in the middle crust to be S_iS, the converted phase would arrive ≥ 3.0 s earlier than observed. Alternatively, if such a conversion occurred in the near surface off the sediment-basement interface, the converted phase would be separated from S_iS by 0.2–0.3 s. This separation is less than the separation between calculated travel time curves for Poisson's ratios of 0.22 and 0.23. Consequently, if a near-surface converted phase is identified as S_iS, the error in our calculated Poisson's ratio is ≤ 0.01. Finally, if we've interpreted *SmS* to be S_iS, Poisson's ratio is over estimated by

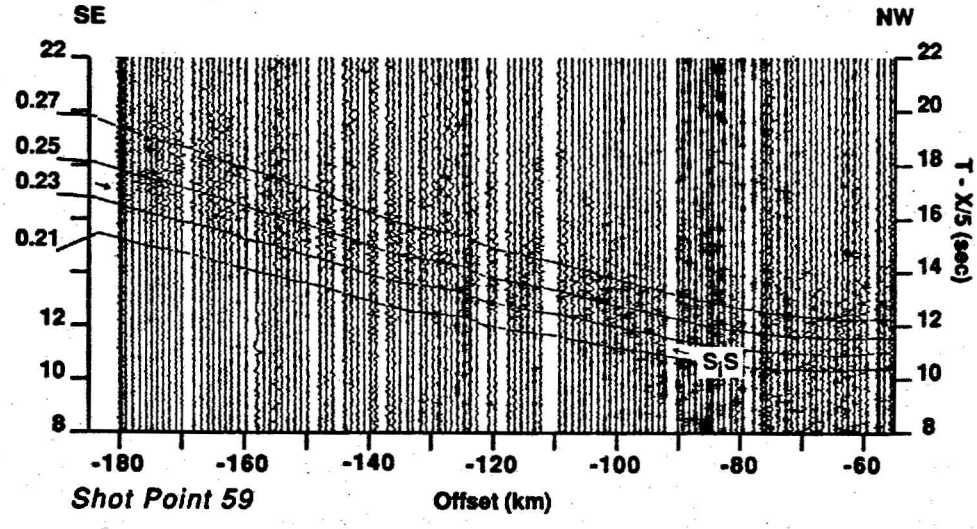

Fig. 11. S_iS recorded from shot point 59. The data are plotted in trace normalized format with a reduction velocity of 5.0 km/s. S_iS calculated travel times for several values of Poisson's ratio (labeled on the left) are overlain.

0.03–0.04. However, a similar velocity gradient modeled in layer 6 for compressional waves would be expected for shear waves, focusing SmS to a smaller range of offsets than observed for S_iS in these data.

Discussion

Surface Geology and the Velocity Model

The limited lateral velocity variability of the model (Figure 8*b*) is suggestive of a mineralogically homogeneous medium. The bedrock of the southern YTT consists of metasedimentary and metagranitic rocks and granitic plutons. Since shear wave and compressional wave velocities relate to mineralogy [*Christensen*, 1966*a*; *Christensen and Fountain*, 1975; *Kern and Richter*, 1981] and representative YTT samples along the profile consist mainly of varying proportions of quartz, sodic plagioclase, and mica (Table 1) which have similar average compressional wave velocities [*Babuška*, 1981], compressional wave velocities are expected to be relatively uniform along the profile (Figure 12). Consequently, although the bedrock geology is complex (Figure 8*a*), the seismic structure is simple (Figure 8*b*). The shallow extent of both the Shaw Creek fault and the sillimanite gneiss dome in the velocity model can be explained by this lack of velocity discrimination between the bedrock units along the profile. However, previous refraction studies across gneiss domes [e.g., *Mooney et al.*, 1985] indicate deep-rooted velocity structures, suggesting the possibility that the sillimanite gneiss dome along this profile could alternatively be truncated at depth.

Crustal Composition Beneath the YTT

Concurrent analysis of compressional and shear wave data can be used to constrain crustal lithologies [e.g., *Holbrook et al.*, 1988]. Poisson's ratio, calculated from compressional and shear wave velocities, yields more information than either velocity alone. The modulus's dependence on modal composition and the influence of several key minerals is well known [*Christensen*, 1966*b*; *Christensen and Fountain*, 1975; *Kern and Richter*, 1981]. Quartz imposes the greatest influence on a rock's Poisson's ratio; quartz has an anomalously low ratio of 0.08 due to a low compressional wave velocity and high shear wave velocity [*Christensen and*

TABLE 1. Modal Composition of YTT Samples

	Sample			
	TA-42	TA-44	TA-46	TA-47
Rock type	feldspathic quartz mica gneiss	quartz mica schist	sillimanite gneiss	quartz feldspar gneiss
Metamorphic grade	amphibolite	amphibolite	upper amphibolite	amphibolite
	Percent Volume			
Mineral				
Quartz	32	70	65	55
Plagioclase	40	5	6	40
Muscovite	12	20	25	...
Biotite	8	2	2	1
Garnet	3	3	...	2
Microcline	5	...	...	...
Magnetite	...	...	1	2
Sillimanite	...	...	1	...

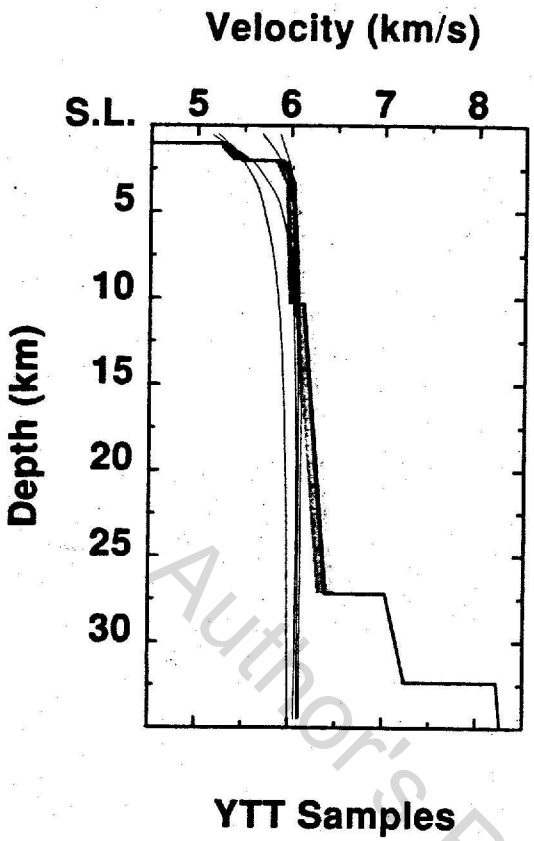

Fig. 12. A comparison of our average Yukon-Tanana terrane (YTT) velocity function (thick line) with laboratory measured velocities (thin lines) for four YTT samples. The shaded region from 2 to 27 km depth represents ±0.1 km/s. The laboratory velocities have been temperature corrected using a geotherm for a surface heat flow of 40 mW/m^2. See Table 1 for sample compositions.

Fountain, 1975]. Other rock-forming minerals have Poisson's ratios between 0.2 and 0.4 [see *Christensen and Fountain*, 1975]. Our determination of a Poisson's ratio of 0.23 for depths of ≤ 27 km indicates a silicic bulk crustal composition beneath the YTT and is in agreement with the Poisson's ratio determined by *Hanson et al.* [1968].

By comparing our velocity model to laboratory measured velocities we can further constrain likely crustal compositions beneath the Fairbanks South deployment (Figure 13; Table 2). In order to make a proper comparison, laboratory velocities need to be corrected for temperature. For our comparison, we use a standard geotherm for a surface heat flow of 40 mW/m^2. We use a geotherm for this value as opposed to one for the surface heat flow measured by *Lawver et al.* [1981] for two reasons. First, the high *Pn* recorded by the Fairbanks South deployment suggests low temperatures at the base of the crust [*Black and Braile*, 1982]. For regions with heat flow similar to that of the YTT (e.g., Basin and Range), mean *Pn* velocities are 7.8–8.0 km/s [*Black and Braile*, 1982]. This argument, however, is complicated by the possibility of upper mantle anisotropy. Second, the earthquake focal depths determined by *Gedney et al.* [1980] indicate brittle deformation to depths of approximately 20 km beneath the YTT, suggesting a lower geotherm than expected from the surface heat flow [*Sibson*, 1984]. The high heat flow measured in the Eilson pluton [*Lawver et al.*, 1981] can be accounted for by the inferred felsic crustal composition, based on the low crustal velocities, beneath the YTT. Typical geotherms are calculated assuming a decrease in the concentration of radiogenic elements in the crust with depth [*Lachenbruch*, 1970]. We propose that the YTT overall felsic crustal composition provides a more even distribution of radiogenic elements throughout the crust. Therefore the high heat flow measured at the Eilson pluton is explained by a higher than normal crustal contribution affording a lower temperature gradient throughout the crust.

Temperature-corrected velocities measured from representative samples collected along the Fairbanks South deployment match the average YTT velocity structure to within ±0.1 km/s to depths of approximately 10 km (Figure 12). Poisson's ratio for these samples range from 0.22 to 0.24. Also fitting the average YTT velocity structure between 0 and 10 km in depth are laboratory velocities for granites (Figure 13*a*). From 10 to 27 km in depth, intermediate to felsic lithologies are compatible with the average YTT middle and lower crustal velocity structure (Figures 13*a* and 13*b*). In contrast, mafic lithologies grossly misfit the low (≤ 6.4 km/s) YTT middle to lower crustal velocities (Figures 13*c* and 13*d*). At the base of the crust (27–31 km), layer 6 is well matched by laboratory velocities for gabbro and amphibolite (Figures 13*c* and 13*d*). These comparisons indicate that the YTT surface lithologies extend up to 10 km in depth. This result is in agreement with geological and geophysical evidence that the YTT is a thin-skinned (≤ 10 km thick) terrane. Beneath the YTT proper, the crust has a high silica, felsic composition. We note that the interpreted, tectonically underplated and presumably metamorphosed Mesozoic flysch proposed by *Stanley et al.* [1990] would have a similar, high silica, felsic composition and therefore would also be expected to fit the midcrustal to lower crustal velocity function (Figure 13*f*). Preliminary laboratory-measured velocities on Kahiltna terrane flysch are in agreement with this interpretation. Based on velocity alone, the base of the crust, layer 6 in the velocity model, marks a lithologic change from felsic lower crust to a more mafic composition. Had we used a higher geotherm, the temperature-corrected laboratory velocities would be approximately 0.1–0.2 km/s lower and would still support the above conclusions.

The origin of the thin, high-velocity layer at the base of the crust beneath the YTT remains enigmatic. Possible candidates for this basal layer include a magmatically underplated mafic layer, a thinned remnant of oceanic crust, a high-grade metamorphic equivalent of the crust overlying it, a relic of continental margin lower crust, or an underplated part of the Wrangellia terrane. Based on the refraction results and laboratory velocities, we can only rule out one of these candidates. A comparison of laboratory velocities for both silicic and felsic granulites (Figure 13*f*) indicates that a high-grade metamorphic equivalent of our interpreted lower crust would not satisfy the YTT velocity function.

Comparisons to Velocity Structures From Other Regions

A somewhat similar Mesozoic and Cenozoic geologic history is shared by the YTT and the southwestern Basin and Range. This history includes outboard accretion, compression and plutonism, followed by extension. Refraction and wide-angle reflection data from the southwestern Basin and Range resemble those of the YTT; *Pg* is near 6.0 km/s, P_iP

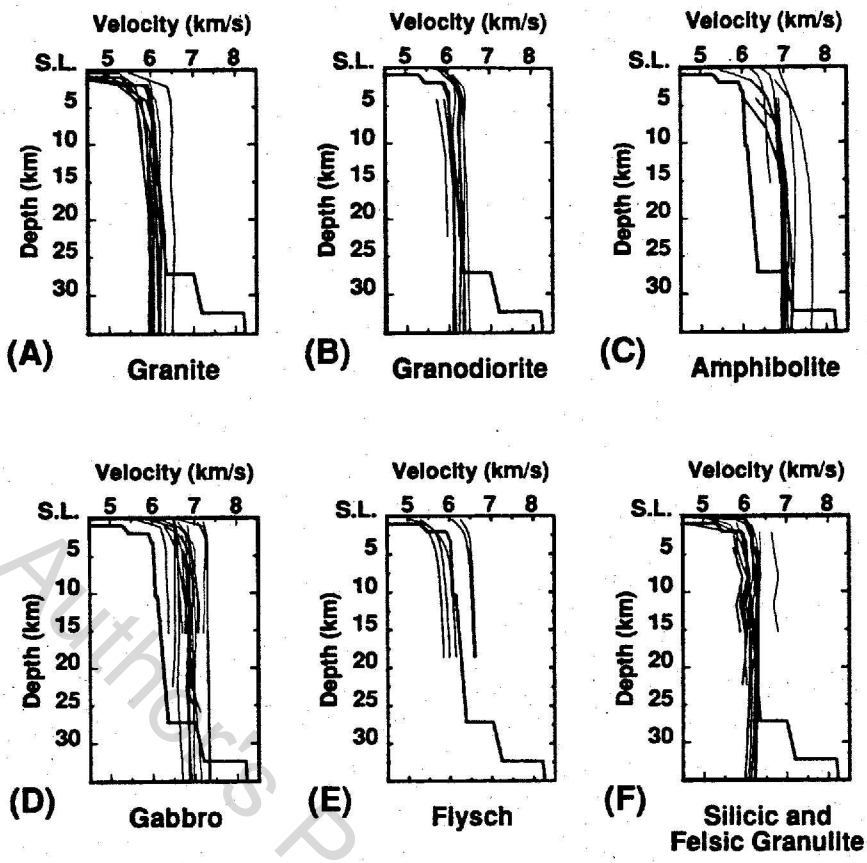

Fig. 13. A comparison of our average Yukon-Tanana terrane (YTT) velocity function (thick line) with laboratory measured velocities (thin lines) for six rock types. The laboratory velocities have been temperature corrected using a geotherm for a surface heat flow of 40 mW/m^2. See Table 2 for sources of laboratory measurements. (*a*) YTT compared to 15 granite samples. (*b*) YTT compared to 10 granodiorite samples. (*c*) YTT compared to 11 amphibolite samples. (*d*) YTT compared to 33 gabbro samples. (*e*) YTT compared to six flysch samples. (*f*) YTT compared to 19 silicic and felsic granulite samples.

is visible, and *PmP* is clear in most places. We compare the YTT velocity structure to the velocity structure for the Buckskin-Rawhide metamorphic core complex of southwestern Arizona [*McCarthy and Thompson*, 1988] (Figure 14*a*). Like the YTT, this region has surface exposures of midcrustal rocks. The Buckskin-Rawhide metamorphic core complex of southwestern Arizona exhibits a similar low-velocity crust as the YTT (average velocities of 6.1 and 6.3 km/s for the YTT and Buckskin-Rawhide profiles, respectively) [*McCarthy and Thompson*, 1988] (Figure 14*a*). Differences between these two velocity structures occur in the upper 3 km of crust, where the Buckskin-Rawhide metamorphic core complex has significantly higher velocities, and at the base of the crust, where the YTT exhibits a higher-velocity lower crustal layer, a deeper Moho by 4 km, and a higher upper mantle velocity. Unlike the Buckskin-Rawhide

TABLE 2. References for Laboratory Velocities

Rock Type	Reference
Amphibolite	*Brooks* [1985], *Christensen* [1966*a*], *Fountain* [1976], *Kanamori and Mizutani* [1965], and *Simmons* [1964]
Flysch	*Fuis et al.*, [1991]
Granite	*Birch* [1961], *Bonner and Schock* [1981], *Brooks* [1985], *Hall and Simmons* [1979], *Kern and Schenk* [1985], *Schock et al.* [1974], *Simmons and Brace* [1965], and *Simmons* [1964]
Gabbro	*Bonner and Schock* [1981], *Brooks* [1985], *Christensen* [1978], *Christensen et al.* [1973], *Chroston and Evans* [1983], *Fox et al.* [1973], *Hyndman* [1976], *Kanamori and Mizutani* [1965], *Kroenke et al.* [1976], and *Nur and Simmons* [1969]
Granodiorite	*Bonner and Schock* [1981], *Brooks* [1985], *Christensen* [1978], *Kanamori and Mizutani* [1965], *Kern and Schenk* [1985], and *Schock et al.* [1974]
Silicic and felsic granulite	*Bonatti and Seyler* [1987], *Christensen and Fountain* [1975], *Chroston and Brooks* [1989], *Hall and Simmons* [1979], *Kern and Schenk* [1985, 1988], and *Manghnani et al.* [1974]

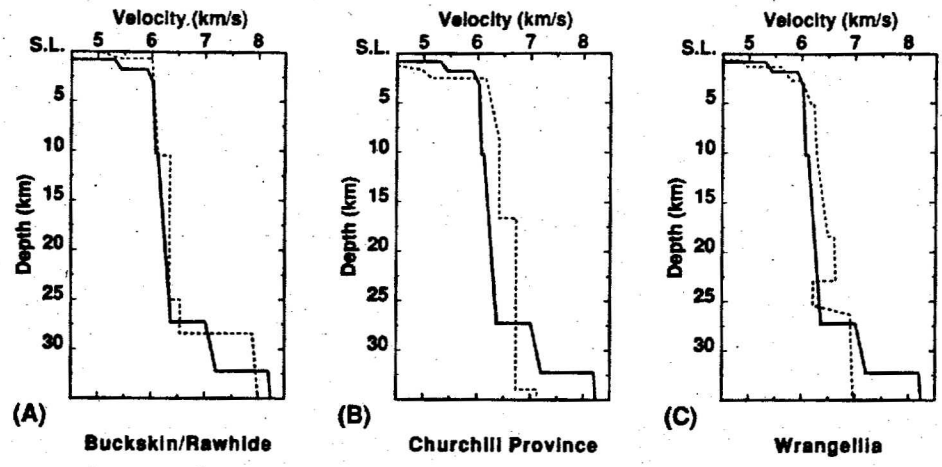

Fig. 14. The velocity structure of the Yukon-Tanana terrane (solid line) compared to the velocity structures from several regions. (*a*) The Buckskin/Rawhide metamorphic core complex, southwestern Arizona [*McCarthy and Thompson*, 1988]. (*b*) The Churchill province, south central Saskatchewan, Canada [*Hajnal et al.*, 1984]. (*c*) The Wrangellia terrane, southeastern Alaska [*Goodwin et al.*, 1989].

model, the basal high-velocity layer in our model fits well within the velocity range for mantle-derived rocks [*Furlong and Fountain*, 1986]. Recent work by *Kushiro* [1990] suggests that partial melting of the mantle wedge is a viable mechanism for crustal underplating in a subduction zone setting. In *Kushiro*'s [1990] model, the base of island arc crust consists of mafic cumulates juxtaposed with ultramafic cumulates (including olivine pyroxenite), a boundary which would seismically be defined as Moho. This model provides an alternative explanation for the high *Pn* velocity beneath the YTT. A high percentage of olivine in the upper mantle, as opposed to a low upper mantle temperature, can explain the high *Pn* velocity; olivine exhibits relatively little variation in velocity with temperature [*Christensen*, 1979].

Early models suggest that the YTT was emplaced or constructed on continental crust [*Tempelman-Kluit*, 1976; *Dusel-Bacon and Aleinikoff*, 1985; *Mortensen and Jilson*, 1985], similar to that of the Canadian shield in the Churchill province [*Dusel-Bacon and Aleinikoff*, 1985]. The more recent model of *Stanley et al.* [1990] indicates that the crust beneath the underplated Mesozoic flysch could possibly be a part of the Wrangellia terrane. Here we compare the YTT velocity structure to both continental crust [*Hajnal et al.*, 1984] (Figure 14*b*) and the Wrangellia terrane [*Goodwin et al.*, 1989] (Figure 14*c*). The significantly higher velocities (0.3–0.6 km/s higher) observed for the Churchill province [*Hajnal et al.*, 1984] in the upper to lower crust as compared to the YTT (between 5 and 27 km in depth) indicates that these rocks can no longer exist beneath the YTT (Figure 14*b*). The comparison between the velocity structure of the YTT and the Wrangellia terrane presents a more complicated picture (Figure 14*c*). Taking into account changes in velocity due to confining pressure and temperature, midcrustal (between 10 and 20 km in depth) velocities for the Wrangellia terrane [*Goodwin et al.*, 1989] are consistent with midcrustal to lower crustal (layer 5 from 15 to 27 km in depth) velocities in the YTT velocity model. Additionally, the high (6.9 km/s) lower crustal (≥ 26 km in depth) velocities observed for the Wrangellia terrane match the velocities for layer 6 in our YTT model. These two observation allow the possibilities that either the lower part of layer 5 or layer 6 is an underplated part of the Wrangellia terrane.

A Model of Crustal Growth for the YTT

The origin of the crust beneath the YTT is a complex problem. Common Pb isotopic studies [*Nokleberg and Lange*, 1985; *Aleinikoff et al.*, 1986, 1987], initial Sr ratios [*Le Couteur and Tempelman-Kluit*, 1976; *Dusel-Bacon and Aleinikoff*, 1985; *Mortensen and Jilson*, 1985; *Aleinikoff et al.*, 1986], and U-Pb ages on relict detrital zircons [*Aleinikoff et al.*, 1986, 1987] support a continental affinity for the YTT. In contrast, magnetotelluric studies indicate the middle to lower crustal rocks beneath the YTT are highly conductive, tectonically underplated Mesozoic flysch and other conductive units [*Labson et al.*, 1988; *Stanley et al.*, 1990]. Also bearing on this is the recent work of *Aleinikoff et al.* [1989, 1990] that indicates progressive contamination of Cretaceous and early Tertiary granitic magmas by rocks with the same range of isotopic ratios as the Mesozoic flysch from the Kahiltna terrane and the Gravina arc. With these observations and our determination of a thin, silicic crust beneath the YTT, we propose the following interpretation of this crustal structure: (1) The YTT was originally formed on continental crust [*Dusel-Bacon and Aleinikoff*, 1985; *Mortensen and Jilson*, 1985; *Nokleberg et al.*, 1989]. (2) During initial amalgamation and subsequent translation the YTT's continentally derived upper crust was telescoped, thereby forming a largely sialic crustal section. (3) Subsequently, the YTT was tectonically underplated by Mesozoic flysch with the ancestral YTT middle to lower crust being tectonically eroded [*Stanley et al.*, 1990]. (4) The collision and amalgamation of Wrangellia, as part of the Peninsular-Alexander-Wrangellia superterrane, emplaced a portion of Wrangellia beneath the YTT/Mesozoic flysch assemblage. (5) Continued outboard subduction and related magmatism underplated the YTT assemblage with mantle-derived mafic rocks.

CONCLUSIONS

Our tectonic model depicts the formation of the interpreted crustal structure beneath the southern YTT. The

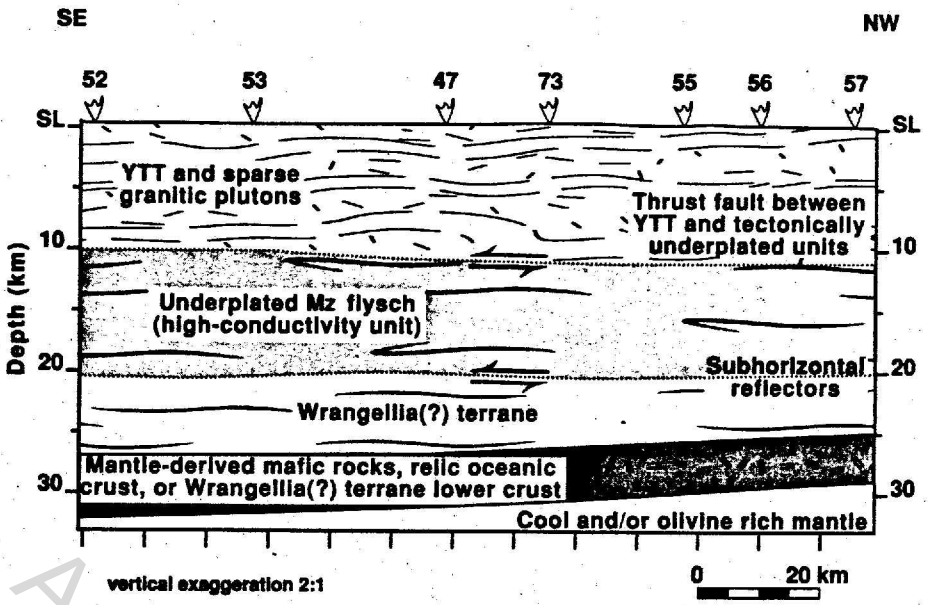

Fig. 15. Interpretive cross section of the crust beneath the Yukon-Tanana terrane.

main features of the crustal structure are (Figure 15): the low-velocity rocks of the southern YTT extend from the surface to depths of about 10 km; a décollement, approximately interface "A", at the base of the southern YTT; the occurrence beneath the southern YTT of the underthrusted Mesozoic flysch and basement of the Wrangellia(?) terrane; low-velocity rocks extending to depths of about 27 km; a 3- to 5-km-thick layer of mantle-derived mafic rocks, relic oceanic crust, or Wrangellia(?) terrane lower crust extend from 27 km to approximately 30 km in depth; a tectonically young Moho beneath the southern YTT at an average depth of 30 km; and mantle that may be relatively cool and/or olivine rich.

The deep-crustal structure beneath the YTT is interpreted as forming by various events including underthrusting and tectonic erosion, underplating of mafic magma and extension during Mesozoic time. Associated with the emplacement of the lower crust, intense subhorizontal fabric formed during multiple periods of low-angle thrusting and extensional faulting. This fabric is manifest in the reflectivity at middle to lower crustal depths observed in the refraction data. The Moho is interpreted as a tectonically young feature forming either during the emplacement of mantle-derived magmas or the underthrusting of the Wrangellia terrane. Finally, the Fairbanks South refraction data confirm that the Yukon-Tanana terrane accreted via thin-skinned tectonics and that underplating by subducting sediments has played a significant role in crustal growth for central Alaska.

Acknowledgments. We wish to thank Thomas Brocher, Robert Hawman, Jill McCarthy, and Anne Trehu for insightful reviews and suggestions which helped improve this manuscript. Erik Goodwin, Steve Holbrook, Craig Jarchow, Stan Ruppert, and John Howie provided perceptive discussions throughout the progress of this research. In addition we would like to thank the sponsors of the Stanford Exploration Project whose support helps maintain the CONVEX computer used to generate the synthetic seismograms. We gratefully acknowledge the assistance in our field work and initial data processing by Elizabeth Ambos, Patricia Berge, Robert Colburn, Charles Collum, George Corbin, Joseph Cotton, Ernst Flueh, Liz Green, Ronald Kaderabek, William Kohler, Robert Luzitano, Robert McClearn, Janice Murphy, Benjamin Page, David Reneau, Scott Schapper, Julie Shemeta, John Van Schaack, Dean Whitman, and Jeffrey Wilson. We especially wish to thank Edward Criley, who supervised field operations. We are indebted to our Canadian colleagues Timothy Cote, Terry Neufeld, and Carl Spencer for graciously contributing 20 instruments to our experiments, operating the instruments, and reducing the data. We also wish to thank our colleagues at the University of Alaska at Fairbanks, David Stone, John Davies, and Lorraine Wolf, who kindly allowed us to house our computer at their university. The laboratory studies were supported by the Office of Naval Research contract N00014-89-J-1209.

REFERENCES

Aleinikoff, J. N., and W. J. Nokleberg, Age of Devonian igneous-arc terranes in the northern Mount Hayes quadrangle, eastern Alaska Range, *U.S. Geol. Surv. Circ.*, *967*, 44–49, 1985.

Aleinikoff, J. N., C. Dusel-Bacon, and H. L. Foster, Geochronology of augen gneiss and related rocks, Yukon-Tanana terrane, east-central Alaska, *Geol. Soc. Am. Bull.*, *97*, 626–637, 1986.

Aleinikoff, J. M., C. Dusel-Bacon, H. L. Foster, and W. J. Nokleberg, Pb-isotope fingerprinting of tectonostratigraphic terranes, east-central Alaska, *Can. J. Earth Sci.*, *24*, 2089–2098, 1987.

Aleinikoff, J. N., W. D. Stanley, and W. J. Nokleberg, Pb isotope evidence for underthrusted Mesozoic flysch beneath the Yukon-Tanana terrane, east-central Alaska (abstract), *Eos Trans. AGU*, *70*, 1337, 1989.

Aleinikoff, J. N., C. Dusel-Bacon, H. L. Foster, and W. J. Nokleberg, A summary of isotopic constraints on the history of the Yukon-Tanana terrane, east-central Alaska (abstract), *Geol. Assoc. Can. Abstr. Program*, *15*, A1, 1990.

Babuška, V., Anisotropy of *vp* and *vs* in rock-forming minerals, *J. Geophys.*, *50*, 1–6, 1981.

Banda, E., N. Deichmann, L. W. Braile, and J. Ansorge, Amplitude study of the *Pg* phase, *J. Geophys.*, *51*, 153–164, 1982.

Barnes, D. F., Bouguer gravity anomaly map of Alaska, scale 1: 2500000, *U.S. Geol. Surv. Geophys. Invest. Map*, *GP-913*, 1977.

Beaudoin, B. C., G. Perkins, and G. S. Fuis, Data report for the TACT 1987 seismic refraction survey: Alaska Range and Fairbanks south deployments, *U.S. Geol. Surv. Open File Rep.*, *89-321*, 1989.

Birch, F., The velocity of compressional waves in rocks to 10 kilobars, part 2, *J. Geophys. Res.*, *66*, 2199–2224, 1961.

Black, P. R., and L. W. Braile, Pn velocity and cooling of the

continental lithosphere, *J. Geophys. Res.*, *87*, 10,557–10,568, 1982.

Bonatti, E., and M. Seyler, Crustal underplating and evolution in the Red Sea Rift: Uplifted gabbro/gneiss crustal complexes of Zabargad and Brothers Islands, *J. Geophys. Res.*, *92*, 12,803–12,821, 1987.

Bonner, B. P., and R. N. Schock, Seismic wave velocity, in *Physical Properties of Rocks and Minerals*, edited by Y. S. Touloukian, W. R. Judd and R. F. Roy, pp. 221–256, McGraw-Hill, New York, 1981.

Braile, L. W., and C. S. Chiang, The continental mohorovičić discontinuity: Results from near-vertical and wide-angle seismic reflection studies, in *Reflection Seismology: The Continental Crust*, *Geodyn. Ser.*, vol. 13, edited by M. Barazangi and L. Brown, pp. 257–272, AGU, Washington, D. C., 1986.

Brocher, T. M., M. A. Fisher, E. L. Geist, and N. I. Christensen, A high-resolution seismic reflection/refraction study of the Chugach-Peninsular terrane boundary, southern Alaska, *J. Geophys. Res.*, *94*, 4441–4455, 1989.

Brooks, S. G., Seismic velocities from crustal sections in northern Scandinavia, Ph.D. thesis, Univ. of East Anglia, Norwich, England, 1985.

Campbell, D. L., Profiles showing models of magnetic structures in accreted terranes of south-central Alaska, scale 1: 500000, *U.S. Geol. Surv. Misc. Geol. Invest. Map*, *MF-1912*, 1987.

Campbell, D. L., and W. J. Nokleberg, Magnetic model of a profile across northern Copper River Basin, northeastern Gulkana quadrangle, *U.S. Geol. Surv. Circ.*, *978*, 35–38, 1986.

Červený, V., I. A. Molotkov, and I. Pšenčík, *Ray Method in Seismology*, 214 pp., University of Karlova, Prague, 1977.

Christensen, N. I., Compressional wave velocities in metamorphic rocks at pressures to 10 kilobars, *J. Geophys. Res.*, *70*, 6147–6164, 1965.

Christensen, N. I., Shear wave velocities in metamorphic rocks at pressures to 10 kilobars, *J. Geophys. Res.*, *71*, 3549–3556, 1966*a*.

Christensen, N. I., Elasticity of ultrabasic rocks, *J. Geophys. Res.*, *71*, 5921–5931, 1966*b*.

Christensen, N. I., Ophiolites, seismic velocities and oceanic crustal structure, *Tectonophysics*, *47*, 131–157, 1978.

Christensen, N. I., Compressional wave velocities in rocks at high temperatures and pressures, critical thermal gradients, and crustal low-velocity zones, *J. Geophys. Res.*, *84*, 6849–6857, 1979.

Christensen, N.I., and D. M. Fountain, Constitution of the lower continental crust based on experimental studies of seismic velocities in granulite, *Geol. Soc. Am. Bull.*, *86*, 227–236, 1975.

Christensen, N. I., R. H. Carlson, M. H. Salisbury, and D. M. Fountain, Elastic wave velocities in volcanic and plutonic rocks recovered on DSDP leg 31, *Initial Rep. Deep Sea Drill. Proj.*, *31*, 607–609, 1973.

Chroston, P. N., and S. G. Brooks, Lower crustal seismic velocities from Lofoten-Vesterålen, North Norway, *Tectonophysics*, *157*, 251–269, 1989.

Chroston, P. N., and C. J. Evans, Seismic velocities of granulites from the Seiland Petrographic Province, N. Norway: Implications for Scandinavian lower continental crust, *J. Geophys.*, *52*, 14–21, 1983.

Churkin, M., Jr., H. L. Foster, and R. M. Chapman, Terranes and suture zones in east central Alaska, *J. Geophys. Res.*, *87*, 3718–3730, 1982.

Coney, P. J., D. L. Jones, and J. W. H. Monger, Cordilleran suspect terranes, *Nature*, *288*, 329–333, 1981.

Dusel-Bacon, C., and J. N. Aleinikoff, Petrology and tectonic significance of augen gneiss from a belt of Mississippian granitoids in the Yukon-Tanana terrane, east central Alaska, *Geol. Soc. Am. Bull.*, *96*, 411–425, 1985.

Dusel-Bacon, C., and H. L. Foster, A sillimanite gneiss dome in the Yukon Crystalline terrane, east-central Alaska: Petrography and garnet-biotite geothermometry, *U.S. Geol. Surv. Prof. Pap.*, *1170E*, 1983.

Fisher, M. A., T. M. Brocher, W. J. Nokleberg, G. Plafker, and G. L. Smith, Seismic reflection images of the crust of the northern part of the Chugach terrane, Alaska: Results of a survey for the Trans-Alaska Crustal Transect (TACT), *J. Geophys. Res.*, *94*, 4424–4440, 1989.

Foster, H. L., and T. E. C. Keith, Ultramafic rocks of the Eagle quadrangle, east-central Alaska, *J. Res. U.S. Geol. Surv.*, *2* 657–669, 1974.

Foster, H. L., T. E. C. Keith, and W. D. Menzie, Geology of east-central Alaska, *U.S. Geol. Surv. Open File Rep.*, *87-188*, 1987.

Fountain, D. M., The Ivrea-Verbano and Strona-Ceneri zones, northern Italy: A cross-section of the continental crust—New evidence from seismic velocities of rock samples, *Tectonophysics*, *33*, 145–165, 1976.

Fox, P. J., E. Schreiber, and J. J. Peterson, The geology of the ocean crust: Compressional wave velocities of oceanic rocks, *J. Geophys. Res.*, *78*, 5155–5172, 1973.

Fuchs, K., Synthetic seismograms of *PS*-reflections from the transition zones computed with the reflectivity method, *J. Geophys.*, *41*, 445–462, 1975.

Fuchs, K., and G. Müller, Computation of synthetic seismograms with the reflectivity method and comparison with observations, *Geophys. J. R. Astron. Soc.*, *23*, 417–433, 1971.

Fuis, G. S., E. L. Ambos, W. D. Mooney, N. I. Christensen, and E. Geist, Crustal structure of accreted terranes in southern Alaska, Chugach Mountains and Copper River basin, from seismic refraction results, *J. Geophys. Res.*, *96*, 4187–4227, 1991.

Furlong, K. P., and D. M. Fountain, Continental crustal underplating: Thermal considerations and seismic-petrologic consequences, *J. Geophys. Res.*, *91*, 8285–8294, 1986.

Gedney, L., S. Estes, and N. Biswas, Earthquake Migration in the Fairbanks, Alaska Seismic Zone, *Bull. Seismol. Soc. Am.*, *70*, 223–241, 1980.

Gehrels, G. E., W. C. McClelland, S. D. Samson, P. J. Patchett, and J. L. Jackson, Ancient continental margin assemblage in the northern Coast Mountains, southeast Alaska and northwest Canada, *Geology*, *18*, 208–211, 1990.

Goodwin, E. B., G. S. Fuis, W. J. Nokleberg, and E. L. Ambos, The crustal structure of the Wrangellia terrane along the East Glenn Highway, eastern-southern Alaska, *J. Geophys. Res.*, *94*, 16,037–16,057, 1989.

Griscom, A., Aeromagnetic interpretation of the Big Delta quadrangle, Alaska, *U.S. Geol. Surv. Open File Rep.*, *78-529-B*, 1978.

Hajnal, Z., C. M. R. Fowler, R. F. Mereu, E. R. Kanasewich, G. L. Cumming, A. G. Green, and A. Mair, An initial analysis of the Earth's crust under the Williston Basin: 1979 COCRUST experiment, *J. Geophys. Res.*, *89*, 9381–9400, 1984.

Hall, J., and G. Simmons, Seismic velocities of Lewisian metamorphic rocks at pressures to 8 kbar: Relationship to crustal layering in North Britain, *Geophys. J. R. Astron. Soc.*, *58*, 337–347, 1979.

Hanson, K., E. Berg, and L. Gedney, A seismic refraction profile and crustal structure in central interior Alaska, *Bull. Seismol. Soc. Am.*, *58*, 1657–1665, 1968.

Hawman, R. B., R. H. Colburn, D. A. Walker, and S. B. Smithson, Processing and inversion of refraction and wide-angle reflection data from the 1986 Nevada PASSCAL experiment, *J. Geophys. Res.*, *95*, 4657–4691, 1990.

Healy, J. H., W. D. Mooney, H. R. Blank, M. E. Gettings, W. M. Kohler, R. J. Lamson, and L. E. Leone, Saudi Arabian seismic deep-refraction profile: Final report, *U.S. Geol. Surv. Open File Rep.*, *82-37*, 1982.

Holbrook, W. S., D. Gajewski, A. Krammer, and C. Prodehl, An interpretation of wide-angle compressional and shear wave data in southwest Germany: Poisson's ratio and petrological implications, *J. Geophys. Res.*, *93*, 12,081–12,106, 1988.

Hyndman, R. D., Seismic velocity measurements of basement rocks from DSDP Leg 37, *Initial Rep. Deep Sea Drill. Proj.*, *37*, 373–387, 1976.

Jones, D. L., N. J. Silberling, W. Gilbert, and P. Coney, Character, distribution, and tectonic significance of accretionary terranes in the central Alaska Range, *J. Geophys. Res.*, *87*, 3709–3717, 1982.

Jones, D. L., N. J. Silberling, P. J. Coney, and G. Plafker, Lithotectonic terrane map of Alaska (west of the 141st meridian), scale 1: 2500000, *U.S. Geol. Surv. Misc. Field Stud. Map*, *MF-1874-A*, 1987.

Kanamori H., and H. Mizutani, Ultrasonic measurements of elastic constants of rocks under high pressures, *Bull. Earthquake Res. Inst. Univ. Tokyo*, *43*, 173–194, 1965.

Kern, H., and A. Richter, Temperature-derivatives of compressional and shear wave velocities in crustal and mantle rocks at 6 kbar confining pressure, *J. Geophys.*, *49*, 47–56, 1981.

Kern, H., and V. Schenk, Elastic wave velocities in rocks from a lower crustal section in southern Calabria (Italy), *Phys. Earth Planet. Inter.*, *40*, 147–160, 1985.

Kern, H., and V. Schenk, A model of velocity structure beneath Calabria, southern Italy, based on laboratory data, *Phys. Earth Planet. Inter.*, *87*, 325–337, 1988.

Kroenke, I. W., M. H. Manghnani, C. S. Rai, P. Fryer, and R. Ramananantoandro, Elastic properties of selected ophiolites rocks from Papua, New Guinea: Nature and composition of oceanic lower crust and upper mantle, in *The Geophysics of the Pacific Ocean Basin and Its Margins*, *Geophys. Monogr. Ser.*, vol. 19, edited by G. H. Sutton, M. H. Manghnani, and R. Moberly, pp. 257–272, AGU, Washington, D. C., 1976.

Kushiro, I., Partial melting of mantle wedge and evolution of island arc crust, *J. Geophys. Res.*, *95*, 15,929–15,939, 1990.

Labson, V. F., M. A. Fisher, and W. J. Nokleberg, An integrated study of the Denali fault from magnetotelluric soundings, seismic refraction and geologic mapping (abstract), *Eos Trans. AGU*, *69*, 1457, 1988.

Lachenbruch, A., Crustal temperature and heat production: Implications of the linear heat flow relation, *J. Geophys. Res.*, *75*, 3291–3300, 1970.

Lawver, L. A., A. H. Lachenbruch, and R. J. Munroe, Heat flow in Alaska, in *Physical Properties of Rocks and Minerals*, vol. II-2, edited by Y. S. Touloukian, W. R. Judd, and R. F. Roy, pp. 539–540, McGraw-Hill, New York, 1981.

Le Couteur, P. C., and D. J. Tempelman-Kluit, Rb/Sr ages and a profile of initial Sr^{87}/Sr^{86} ratios for plutonic rocks across the Yukon Crystalline Terrane, *Can. J. Earth Sci.*, *13*, 319–330, 1976.

Luetgert, J. J., Users manual for RAY84/R83PLT: Interactive two-dimensional raytracing/synthetic seismogram package, *U.S. Geol. Surv. Open File Rep.*, *88-238*, 1988.

Lutter, W. J., R. L. Nowack, and L. W. Braile, Seismic imaging of upper crustal structure using travel times from the PASSCAL Ouachita experiment, *J. Geophys. Res.*, *95*, 4621–4631, 1990.

Manghnani, M. H., R. Ramananantoandro, and S. P. Clark, Jr., Compressional and shear wave velocities in granulite facies rocks and eclogites to 10 kbar, *J. Geophys. Res.*, *79*, 5427–5446, 1974.

McCarthy, J., and G. A. Thompson, Seismic imaging of extended crust with emphasis on the western United States, *Geol. Soc. Am. Bull.*, *100*, 1361–1374, 1988.

McMechan, G. A., and W. D. Mooney, Asymptotic ray theory and synthetic seismograms for laterally varying structures and application to the Imperial Valley, California, *Bull. Seismol. Soc. Am.*, *70*, 2021–2035, 1980.

Monger, J. W. H., Cordilleran tectonics: A Canadian perspective, *Bull. Soc. Geol. Fr.*, *26*, 255–278, 1984.

Monger, J. W. H., and H. C. Berg, Lithotectonic terrane map of western Canada and southeastern Alaska, scale 1: 2500000, *U.S. Geol. Surv. Map*, *MF-1874-B*, 1987.

Mooney, W. D., M. E. Gettings, H. R. Blank, and J. H. Healy, Saudi Arabian seismic-refraction profile: A traveltime interpretation of crustal and upper mantle structure, *Tectonophysics*, *111*, 173–246, 1985.

Mortensen, J. K., and G. A. Jilson, Evolution of the Yukon-Tanana terrane: Evidence from southeastern Yukon Territory, *Geology*, *13*, 806–810, 1985.

Murphy, J. M., USGS FM cassette seismic refraction recording system, *U.S. Geol. Surv. Open File Rep.*, *88-570*, 1988.

Nokleberg, W. J., and J. N. Aleinikoff, Summary of stratigraphy, structure, and metamorphism of Devonian igneous-arc terranes, northeastern Mount Hayes quadrangle, eastern Alaska Range, *U.S. Geol. Surv. Circ.*, *967*, 66–71, 1985.

Nokleberg, W. J., and I. M. Lange, Volcanogenic massive sulfide occurrences, Jarvis Creek Glacier subterrane, eastern Alaska Range, Alaska, *U.S. Geol. Surv. Circ.*, *947*, 77–80, 1985.

Nokleberg, W. J., D. L. Jones, and N. J. silberling, Origin and tectonic evolution of the Maclaren and Wrangellia terranes, eastern Alaska Range, Alaska, *Geol. Soc. Am. Bull.*, *96*, 1251–1270, 1985.

Nokleberg, W. J., J. N. Aleinikoff, and I. M. Lange, Cretaceous deformation and metamorphism in the northeastern Mount Hayes quadrangle, eastern Alaska Range, *U.S. Geol. Surv. Circ.*, *978*, 64–69, 1986.

Nokleberg, W. J., H. L. Foster, and J. N. Aleinikoff, Geology of northern Copper River Basin, eastern Alaska Range, and southern Yukon-Tanana Basin, southern and east-central Alaska, in *Alaskan Geological and Geophysical Transect: Field Trip Guideb.*, vol T104, edited by W. J. Nokleberg and M. A. Fisher, pp. 34–63, AGU, Washington, D. C., 1989.

Nur, A., and G. Simmons, The effect of saturation on velocity in low porosity rocks, *Earth Planet. Sci. Lett.*, *7*, 183–193, 1969.

Page, R. A., G. Plafker, G. S. Fuis, W. J. Nokleberg, E. L. Ambos, W. D. Mooney, and D. L. Campbell, Accretion and subduction tectonics in the Chugach Mountains and Copper River Basin, Alaska: Initial results of the Trans-Alaska Crustal Transect, *Geology*, *14*, 501–505, 1986.

Patton, W. W., Jr., S. E. Box, and D. Grybeck, Ophiolites and other mafic-ultramafic complexes in Alaska, scale 1: 5,000,000, *U.S. Geol. Surv. Open File Rep.*, *89-648*, 1989*a*.

Patton, W. W., Jr., S. E. Box, E. J. Moll-Stalcup, and T. P. Miller, Geology of west-central Alaska, *U.S. Geol. Surv. Open File Rep.*, *89-554*, 1989*b*.

Pavlis, T. L., V. B. Sisson, W. J. Nokleberg, G. Plafker, and H. L. Foster, Evidence for Cretaceous crustal extension in the Yukon Crystalline terrane, east-central Alaska (abstract), *Eos Trans. AGU*, *69*, 1453, 1988.

Plafker, G., W. J. Nokleberg, and J. S. Lull, Bedrock geology and tectonic evolution of the Wrangellia, Peninsular, and Chugach terranes along the Trans-Alaska Crustal Transect in the Chugach Mountains and southern Copper River Basin, Alaska, *J. Geophys. Res.*, *94*, 4255–4295, 1989*a*.

Plafker, G., C. D. Blome, and N. J. Silberling, Reinterpretation of lower Mesozoic rocks on the Chilkat Peninsula, Alaska, as a displaced fragment of Wrangellia, *Geology*, *17*, 3–6, 1989*b*.

Schock, R. N., B. P. Donner, and L. Louis, Collection of ultrasonic velocity data as a function of pressure for polycrystalline solids, *Tech. Rep. UCRL-51508*, 262 pp., Lawrence Livermore Lab., Livermore, Calif., 1974.

Sibson, R. H., Roughness at the base of the seismogenic zone: Contributing factors, *J. Geophys. Res.*, *89*, 5791–5799, 1984.

Simmons, G., Velocity of shear waves in rocks to 10 kilobars, 1, *J. Geophys. Res.*, *69*, 1123–1130, 1964.

Simmons, G., and W. F. Brace, Comparison of static and dynamic measurements of compressibility of rocks, *J. Geophys. Res.*, *70*, 5649–5656, 1965.

Stanley, W. D., V. F. Labson, W. J. Nokleberg, B. Csejtey, Jr., and M. A. Fisher, The Denali fault system and Alaska Range of Alaska: Evidence for underplated Mesozoic flysch from magnetotelluric surveys, *Geol. Soc. Am. Bull.*, *102*, 160–173, 1990.

Stout, J. H., J. B. Brady, F. R. Weber, and R. A Page, Evidence for Quaternary movement on the McKinley strand of the Denali fault in the Delta River area, Alaska, *Geol. Soc. Am. Bull.*, *84*, 939–947, 1973.

Tempelman-Kluit, D. J., The Yukon crystalline terrane: Enigma in the Canadian cordillera, *Geol. Soc. Am. Bull.*, *87*, 1343–1357, 1976.

Weber, F. R., H. L. Foster, T. E. C. Keith, and C. Dusel-Bacon, Preliminary geologic map of the Big Delta quadrangle, Alaska, scale 1: 250000, *U.S. Geol. Surv. Open File Rep.*, *78-529A*, 1978.

Wenzel, F., K. Sandmeier, and W. Wälde, Properties of the lower crust from modeling refraction and reflection data, *J. Geophys. Res.*, *92*, 11,575–11,583, 1987.

Woollard, G. P., N. A. Ostenso, E. Thiel, and W. E. Bonini, Gravity anomalies, crustal structure, and geology in Alaska, *J. Geophys. Res.*, *65*, 1021–1037, 1960.

B. C. Beaudoin, Department of Geophysics, Stanford University, Stanford, CA 94305-2215.

N. I. Christensen, Department of Earth and Atmospheric Sciences, Purdue University, West Lafayette, IN 47907.

C. S. Fuis, W. D. Mooney, and W. J. Nokleberg, U.S. Geological Survey, 345 Middlefield Road, MS 977, Menlo Park, CA 94025.

(Received February 11, 1991;
revised September 20, 1991;
accepted October 30, 1991.)